Journal of Asian Earth Sciences 227 (2022) 105093

Contents lists available at ScienceDirect

Journal of Asian Earth Sciences

journal homepage: www.elsevier.com/locate/jseaes

Newly discovered Early Carboniferous and Late Permian magmatic rocks in eastern Myanmar: Implications for the tectonic evolution of the eastern Paleo-Tethys

Fangyang Hu [a,c,d,*], Fu-Yuan Wu [b,c,e], Jian-Gang Wang [b,c,e], Mihai N. Ducea [d,f], James B. Chapman [g], Khin Zaw [h], Wei Lin [b,c,e], Kyaing Sein [i], Sebastien Meffre [h]

[a] Key Laboratory of Mineral Resources, Institute of Geology and Geophysics, Chinese Academy of Sciences, Beijing, China
[b] State Key Laboratory of Lithospheric Evolution, Institute of Geology and Geophysics, Chinese Academy of Sciences, Beijing, China
[c] Innovation Academy for Earth Science, Chinese Academy of Sciences, Beijing, China
[d] Department of Geosciences, University of Arizona, Tucson, AZ, USA
[e] College of Earth and Planetary Sciences, University of Chinese Academy of Sciences, Beijing, China
[f] Faculty of Geology and Geophysics, University of Bucharest, Bucharest, Romania
[g] Department of Geology and Geophysics, University of Wyoming, Laramie, WY, USA
[h] CODES Centre of Ore Deposit and Earth Sciences, University of Tasmania, Hobart, Australia
[i] Myanmar Geosciences Society, Yangon, Myanmar

ARTICLE INFO

Keywords:
Eastern Myanmar
Paleo-Tethys
Magmatic rocks
Petrogenesis
Tectonic evolution

ABSTRACT

Eastern Myanmar is located at the junction of the Changning-Menglian and Chiang Rai-Chiang Mai zone and is a crucial region for constraining the evolution of the eastern Paleo-Tethys. This study presents new zircon U-Pb geochronological, mineral and whole-rock geochemical, and Sr-Nd-Hf-O isotopic data for magmatic rocks from the Sukhothai arc in eastern Myanmar. The rock suites analyzed include 360–355 Ma basaltic rocks and trondhjemitic dikes, and 257–254 Ma volcanic rocks and gabbroic cumulates. The basaltic rocks were derived from partial melting of mélange pair with peridotite and experienced assimilation and fractional crystallization (AFC). The trondhjemitic dikes were formed by partial melting of the basaltic rocks and experienced fractional crystallization at shallow depth. We suggest that andesite and dacite were derived from partial melting of depleted mantle wedge and underwent AFC process. The gabbroic cumulates are a crystallizing phase associated with the melts that produced the coeval volcanic rocks. We propose that eastern Myanmar, Central Tibet, SW Yunnan and Southeast Asia share a similar three-staged magmatic history, forming a ~ 4000 km long magmatic belt. Stage I records the magmatic events related to subduction of the eastern Paleo-Tethys Ocean during the Early Carboniferous. A back-arc basin was opened during the Late Carboniferous, and extensive subduction-related magmatism was followed since the Permian. Stage II records the igneous rocks formed during the final amalgamation between the Indochina and Sibumasu Blocks during the Late Permian to Middle Triassic. Stage III is defined by the post-collisional magmatism distributed across the suture zone during the Late Triassic.

1. Introduction

Understanding the evolution of the Tethys has a great significance for understanding the mechanisms of plate tectonics, paleogeography, metallogeny, and the supercontinental cycle (Deng et al., 2018; Hu et al., 2020; Khin Zaw et al., 2014; Metcalfe, 2013, 2021; Şengör et al., 1984; Wang et al., 2018). Paleo-Tethys, as an important part of the Tethyan history, was interpreted to be the ocean that opened during the Devonian in response to the separation of a series of terranes from northern Gondwana and closed during the Triassic after the continental collision between several terranes from Gondwana and Eurasia (Khin Zaw et al., 2014; Metcalfe, 2013, 2021; Pullen et al., 2008; Şengör et al., 1984; Wang et al., 2018). However, the age of opening, initial subduction, final closure, and the evolutionary history are still hotly debated (Deng et al., 2018; Huang et al., 2018; Metcalfe, 2013; Wang et al., 2017, 2018; Zhao et al., 2018).

* Corresponding author at: Key Laboratory of Mineral Resources, Institute of Geology and Geophysics, Chinese Academy of Sciences, Beijing, China.
E-mail address: hufangyang@mail.iggcas.ac.cn (F. Hu).

https://doi.org/10.1016/j.jseaes.2022.105093
Received 30 October 2021; Received in revised form 4 January 2022; Accepted 5 January 2022
Available online 11 January 2022

Present knowledge about the Paleo-Tethys is largely based on studies of East and Southeast Asia, and therefore the eastern Paleo-Tethys is the focus of this research. The traditional model was that the eastern Paleo-Tethys was opened after the Devonian, and began to subduct during the Early Permian (Deng et al., 2018; Gardiner et al., 2016; Hara et al., 2017; Metcalfe, 2013, 2021; Wang et al., 2018). Recently, some researchers proposed that the eastern Paleo-Tethys may start opening during the Cambrian and subducted from the Late Devonian to the Early Triassic

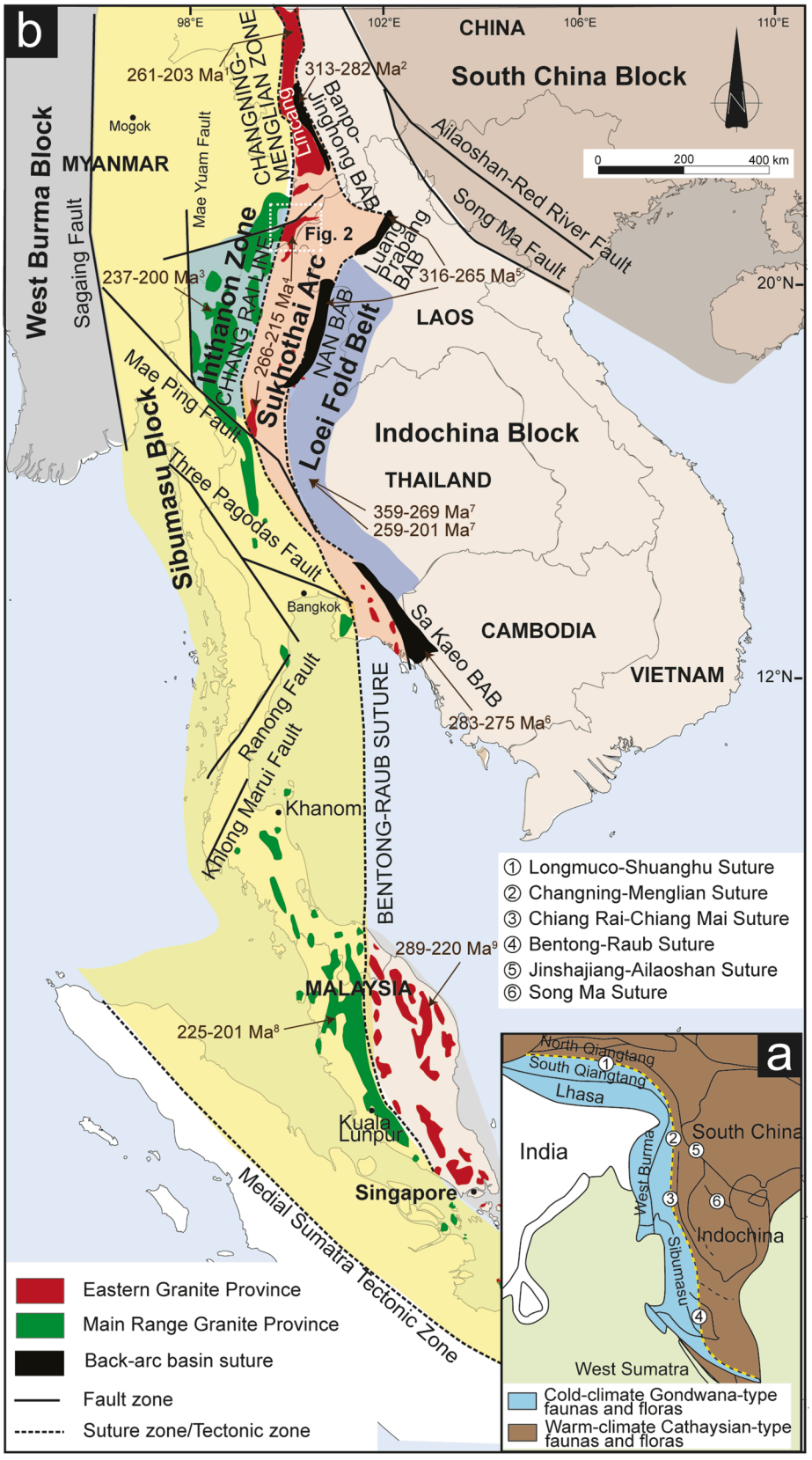

Fig. 1. Simplified map of Southeast Asia showing major tectonic units and their boundaries (modified after Sone and Metcalfe, 2008; Wang et al., 2018; Zhang et al., 2018). The superscripts of formation ages represent different locations: 1, Lincang granite; 2, Banpo-Jinghong back-arc; 3, Main Range Granite Province in Thailand and Myanmar; 4, Eastern Granite Province and Sukhothai arc in Thailand and Myanmar; 5, Luang Prabang-Nan back-arc; 6, Sa Kaeo back-arc; 7, Loid Fold Belt; 8, Main Range Granite Province in Malaysia; 9, Eastern Granite Province in Malaysia. The referenced data are listed in Supplementary Table S1.

based on evidence from the Longmuco-Shuanghu ophiolitic belt (Wang et al., 2017; Zhai et al., 2016, 2018). However, some researchers suggested that the Longmuco-Shuanghu ophiolitic belt was an underthrust metamorphic belt and not an in-situ ophiolitic mélange (Pullen et al., 2008). Silurian ophiolites were found in the Changning-Menglian suture zone, which could have formed during the opening of the Paleo-Tethys Ocean (Wang et al., 2013). To the east of the Changning-Menglian suture, Cambrian-Ordovician ophiolites were recently reported, suggesting that they occurred as the Proto-Tethyan oceanic crust (Liu et al., 2021; Peng et al., 2020; Wei et al., 2022). Detrital zircons documented a "cryptic" magmatic arc during the Late Devonian in southwestern China (Nie et al., 2016), but coeval arc-related magmatic rocks were absent. In the Longmuco-Shuanghu and Changning-Menglian suture zones, Carboniferous granitoids and ophiolites were proposed to have formed in an oceanic arc or continental arc setting related to the subduction of the Paleo-Tethys (Deng et al., 2018; Jian et al., 2009; Liu et al., 2021; Zhai et al., 2016, 2019). In the Jinshajiang segment of the Paleo-Tethys, Carboniferous-Permian rocks were also proposed to be related to the opening and subduction of the Paleo-Tethys (Zi et al., 2012).

In comparison, the pre-Permian arc-related magmatic record of the Paleo-Tethys in Southeast Asia is scarce. Carboniferous mafic rocks were found in northwestern Laos and western Thailand, which were proposed to have formed in a back-arc setting (Khin Zaw and Meffre, 2007; Qian et al., 2016; Shi et al., 2021). However, coeval or earlier arc-related rocks were largely missing resulting in the earlier episodes of the evolution of the Paleo-Tethys in Southeast Asia remaining dubious. As the southern branch of the Paleo-Tethyan arc, the Sukhothai arc preserves important geological records of the amalgamation of the Sibumasu and Indochina Blocks (Gardiner et al., 2016; Hara et al., 2017; Metcalfe et al., 2017; Qian et al., 2015, 2016; Sone et al., 2012; Wang et al., 2016a). Extensive I-type granites and related volcanic rocks (Fig. 1) provide evidence for oceanic subduction along the entire region of the Paleo-Tethys belt (>3000 km) since the Early Permian (Gardiner et al., 2016; Wai-Pan Ng et al., 2015a,b). In consideration of the Early Carboniferous subduction along the Longmuco-Shuangshu and Changning-Menglian suture zones, whether the Paleo-Tethys has a consistent evolutionary history since the Early Carboniferous or gradually younging of initial subduction from the Longmuco-Shuanghu suture to the Chiang Rai-Chiang Mai suture is also still unknown. Thus, identifying early magmatic records in the Sukhothai arc is important for understanding the evolution of the Paleo-Tethys.

In this contribution, we reported the occurrence of newly discovered volcanic-plutonic rocks and cumulates in the Tachileik area, eastern Myanmar. These rocks are distributed in the northern part of the Sukhothai Arc and our new U-Pb zircon dating suggests that they were generated in the Early Carboniferous and Late Permian. Their lithological features, mineral chemistry, whole-rock geochemistry, and whole-rock Sr-Nd isotopic, and zircon Hf-O isotopic compositions indicate that they are products of oceanic subduction. These data fill a temporal gap in the subduction history of the eastern Paleo-Tethys and suggest that oceanic subduction was continuous along a ~ 4000 km long arc system during the Early Carboniferous to Early Triassic along the Paleo-Tethyan belt from western China to SE Asia.

2. Geological background

There are six tectonic units from west to east in Southeast Asia, which are the Sibumasu Block (West Malaya), Inthanon Zone, Chiang Rai-Chiang Mai Suture Zone, Sukhothai arc, Nan-Sa Kaeo back-arc, and the Loei Fold Belt (Indochina Block) (Fig. 1; Hara et al., 2020, 2017; Metcalfe, 2013; Metcalfe et al., 2017). The Sibumasu Block is a combination of multiple micro-blocks including *Si*no (China)-*Bu*rman-*Ma*laysia-*Su*matra, which is a ribbon-like block that originated in northern Gondwana during the Permian (Dew et al., 2018; Zhao et al., 2018). The Sibumasu Block consists of Paleoproterozoic basement and Neoproterozoic to Early Paleozoic siliciclastic and carbonate rocks, and Carboniferous to Permian marine sedimentary rocks (Dew et al., 2018). The Inthanon Zone was proposed to be a fold and thrust belt west of the Chiang Mai-Chiang Rai Suture Zone, which had a basement of the Sibumasu Block (Metcalfe et al., 2017). The Chiang Rai-Chiang Mai Suture Zone (Fig. 1b) contains an accretionary complex that includes mid-ocean ridge basalt (MORB), ocean island basalt (OIB), pelagic chert, limestone, mudstone, and turbidites (Metcalfe, 2013; Metcalfe et al., 2017). The radiolarians from the chert range in age from Middle Devonian to Middle Triassic, bracketing the lifespan of the Paleo-Tethys (Feng, 2002; Feng et al., 2005; Sashida et al., 2000; Sashida and Salyapongse, 2002; Ueno et al., 2010; Wonganan and Caridroit, 2007). The MORB and OIB are correlative with ophiolite blocks formed during 349–307 Ma in the northern Changning-Menglian Suture Zone (Deng et al., 2018; Duan et al., 2006). The back-arc basins (Fig. 1b), including the Banpo-Jinghong, Luang-Prabang, Nan, and Sa Kaeo basins, contains mainly Carboniferous to Early Triassic radiolarian cherts, and Late Carboniferous to Permian basaltic rocks and related ophiolites (Hara et al., 2020; Li et al., 2012; Metcalfe, 2013; Qian et al., 2016; Sone and Metcalfe, 2008; Zhai et al., 2019). The Indochina Block was proposed to be an early-drifted composite block from northern Gondwana during the Early Devonian (Metcalfe, 2013, 2021). It is mainly composed of Paleoproterozoic to Early Paleozoic basement, Mesozoic shallow marine carbonate and siliciclastic rocks, and a Mesozoic to Cenozoic continental red bed sequence (Dew et al., 2018; Wang et al., 2016a). On the western flank of the Indochina Block, the Loei Fold Belt is mainly composed of Devonian-Carboniferous magmatic rocks and Late Permian to Triassic andesitic-rhyolitic volcanic rocks (Kamvong et al., 2014; Khin Zaw and Meffre, 2007; Shi et al., 2021).

The Sukhothai arc is separated from the Loei Fold Belt (Indochina Block) by a series of back-arc basin sutures, including Banpo-Jinghong, Luang Prabang, Nan, and Sa Kaeo back-arc basins (Fig. 1b). These back-arc basins are mainly composed of the Late Carboniferous to Permian ultramafic–mafic complex (peridotite, gabbro, and basalt), and associated limestone and radiolarian chert (Hara et al., 2020; Qian et al., 2016; Sone et al., 2012; Zhai et al., 2019). It is separated from the Sibumasu Block by the Paleo-Tethys suture zones, including the Changning-Menglian Zone, Chiang Mai-Chiang Rai Zone, and Bentong-Raub Zone (Fig. 1b). These Paleo-Tethys suture zones are mainly comprised of Carboniferous to Triassic supra-subduction zone ophiolites, oceanic island basalt (OIB), Devonian to Triassic oceanic radiolarian cherts, limestone blocks, and mélange (Deng et al., 2018; Duan et al., 2006; Jian et al., 2009; Metcalfe, 2013; Metcalfe et al., 2017; Wang et al., 2018; Zhai et al., 2019). The Sukhothai arc was proposed to represent an isolated island arc derived from the Indochina Block with a continental basement (Gardiner et al., 2016; Sone and Metcalfe, 2008). From north to south, the Sukhothai Arc is composed of the Lincang Terrane, Sukhothai Terrane, and Chanthaburi Terrane (Deng et al., 2018; Gardiner et al., 2016; Metcalfe et al., 2017; Sone et al., 2012). The terranes of Sukhothai Arc exposed arc-related I-type granitoids (Eastern Granite Province) and related volcanic rocks, which were mainly formed during the Early Permian to Early Triassic (Cong et al., 2020; Deng et al., 2018; Gardiner et al., 2016; Wai-Pan Ng et al., 2015b). These terranes also contain Permian to Triassic shallow marine sedimentary rocks with warm-water Tethyan type faunas (Hara et al., 2017; Sone et al., 2012; Sone and Metcalfe, 2008). Recent studies showed that the Lincang Batholith was dominated by Triassic S-type granite, which could be correlative with the Main Range Granite Province (Cong et al., 2020; Deng et al., 2018; Gardiner et al., 2016). In this paper, we consider the Lincang Batholith as part of the Eastern Granite Province due to the fact that it is located east of the suture zone, in contrast with the Main Range Granite Province that is distributed to the west of the suture zone.

3. Field occurrence and sampling

The Tachileik area is located in the northern part of the Sukhothai Terrane (Figs. 2 and 3). This area (Fig. 2) is mainly composed of pre-

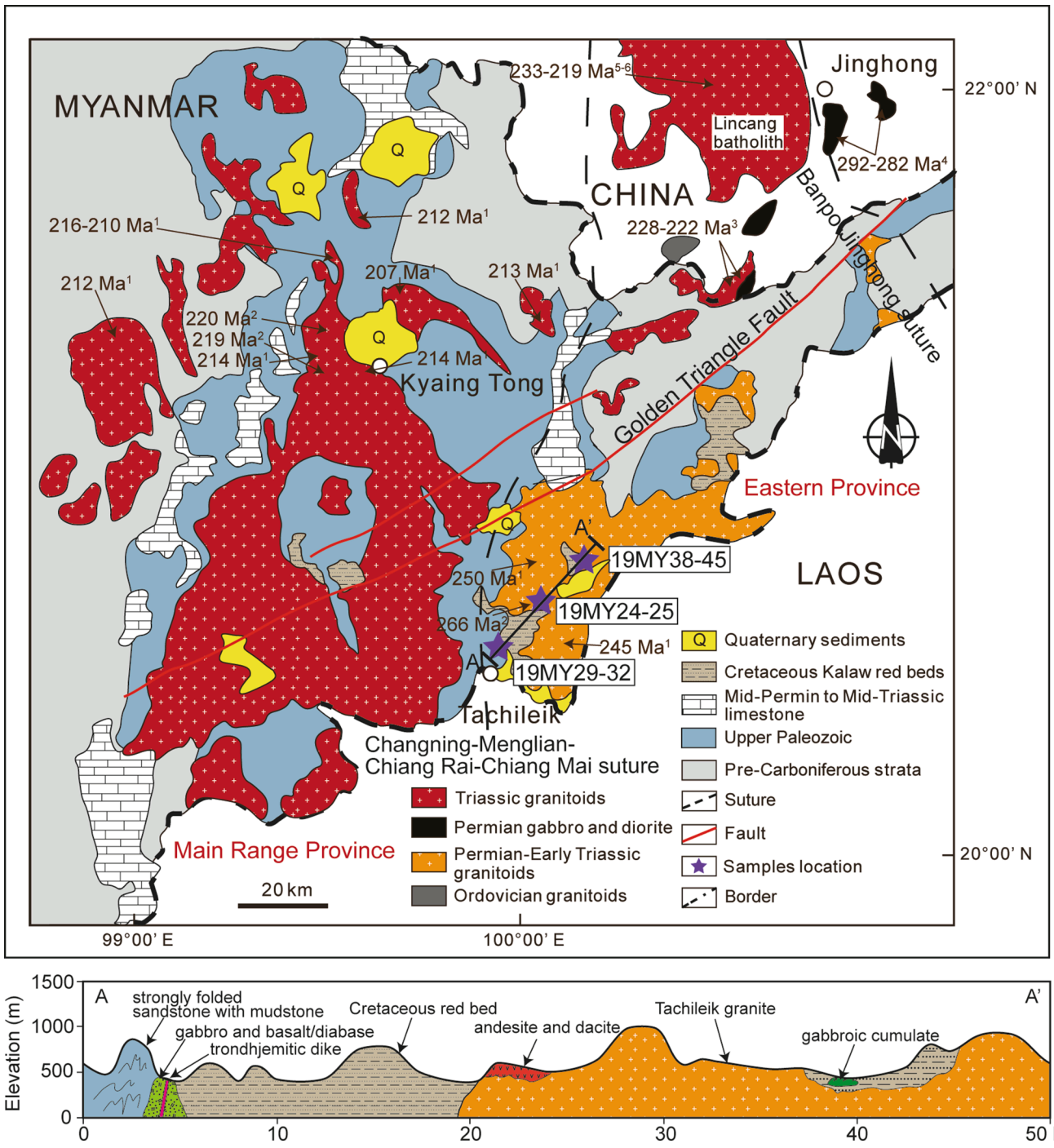

Fig. 2. Simplified geologic map of the Tachileik area, eastern Myanmar (modified after 1:2,250,000 Geologic Map of Myanmar and Metcalfe, 2021) and cross-section profile. The superscripts of formation ages represent source literature: 1, Cong et al. (2021); 2, Gardiner et al. (2016); 3, Wang et al. (2015); 4, Hennig et al. (2009); 5, Wang et al. (2014); 6, Jian et al. (2009).

Carboniferous metasedimentary rocks, Carboniferous sandstone, and Permian to Triassic shale and limestone, which are intruded by the Tachileik Granite (Khin Zaw, 1990). The Tachileik Granite (Fig. 2) belonging to the Eastern Granite Province was emplaced at ~ 266 Ma, and derived from the melting of ancient continental crust during oceanic subduction (Gardiner et al., 2016). To the west of the Tachileik Granite, the Kyaing Tong Granite (Fig. 2) was formed at ~ 220 Ma, belonging to the Main Range Granite Province, and was derived from the melting of ancient continental crust during the continental collision process (Gardiner et al., 2016).

About 3 km north of Tachileik City, an outcrop of weakly to moderately altered mafic assemblages was found, that is basalt/diabase and hornblende gabbro (Fig. 3a). The basalt/diabase is moderately altered and the contact relationship between the hornblende gabbro and basalt/diabase is transitional (Fig. 3a). Additionally, a trondhjemitic dike intruded the hornblende gabbro (Fig. 3b). The hornblende gabbro is medium to fine-grained and consists mainly of hornblende (~58 vol%) and plagioclase (~38 vol%), with an accessory mineral association of zircon, apatite, and magnetite (Fig. 4a). The trondhjemitic dike is porphyritic with quartz and plagioclase phenocrysts and a matrix of quartz, plagioclase, orthoclase, and muscovite with minor zircon and apatite (Fig. 4b).

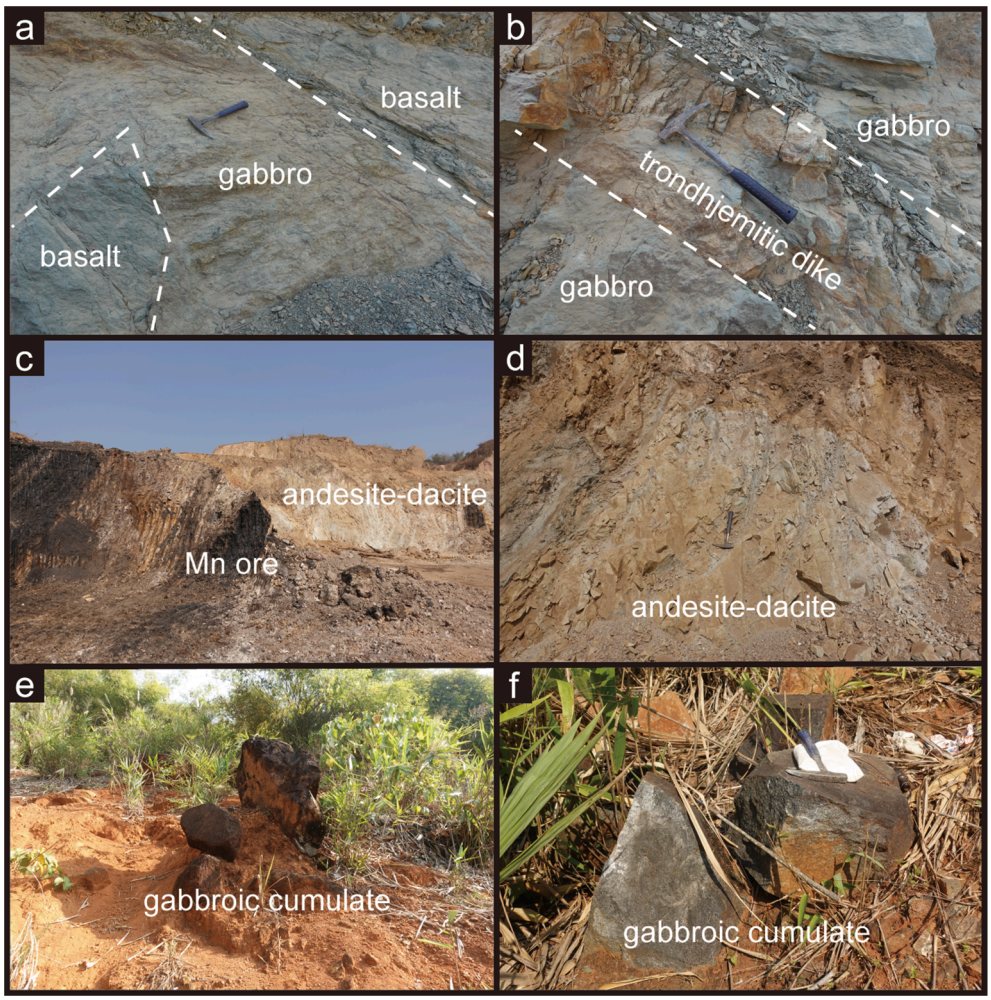

Fig. 3. Outcrop photographs of the magmatic rocks in the Tachileik area showing (a) transitional contact relationship between basalt and gabbro (b) trondhjemitic dike intruding into hornblende gabbro; (c and d) andesite-dacite and related manganese ore deposit; (e and f) gabbroic cumulate.

The Ahr-Ye manganese deposit is located about 20 km northeast of Tachileik City and occurs chiefly in rhyolites and dacites (Fig. 3c and d). The manganese-related ores including cryptomelane, manganite, rhodonite, and braunite occur as layers/veins within these volcanic rocks and associated sedimentary rocks (Minn Chit Thu, 2012; Mitchell, 2018). Intrusion-related gold deposits are also reported in the area (Zaw Myo Htet, 2021). The volcanic rocks experienced varied alteration resulting in chloritization, epidotization, or albitization. The andesite shows medium to fine-grained texture and consists mainly of plagioclase (~58 vol%), hornblende (~35 vol%; altered to chlorite), quartz (~5 vol %), with accessory minerals of zircon, apatite, and magnetite (Fig. 4c). The dacite is porphyritic and plagioclase is the main phenocryst (Fig. 4d). The matrix is mainly composed of fine-grained quartz, plagioclase, and hornblende (altered to chlorite and epidote), with accessory zircon, apatite, and magnetite (Fig. 4d).

About 35 km northeast of Tachileik City, an outcrop of hornblende gabbro and gabbronorite was found (Fig. 3e and f). However, because of the strong weathering and poor exposure, the contact relationship cannot be observed between these gabbroic rocks and other units. The hornblende gabbro and gabbronorite show the massive structure and cumulate texture, which is different from the hornblende gabbro associated with the basalt/diabase mentioned above (Fig. 4e and f). This gabbroic cumulate is composed of orthopyroxene (~0–8 vol%), hornblende (~55–65 vol%), and plagioclase (~25–35 vol%), with accessory mineral assemblages of zircon, apatite, magnetite (Fig. 4e and f).

4. Methods

Whole-rock major and trace elements and whole-rock Sr-Nd isotopes were analyzed at the Wuhan Sample Solution Analytical Technology Co., Ltd., Wuhan, China. Zircon U-Pb-Hf-O isotopic data and major element compositions of minerals were determined at the Institute of Geology and Geophysics, Chinese Academy of Sciences, Beijing, China (IGGCAS). Detailed analytical procedures and instrumental conditions are described in the Supplementary Methods.

5. Results

5.1. Zircon U-Pb ages, and Hf-O isotopes

The zircon U-Pb isotopic data and Hf-O isotopic data for the magmatic rocks from the Tachileik area, eastern Myanmar are given in Supplementary Tables S2 and S3, respectively.

As shown in representative CL images, zircons from different types of rocks show different characteristics (Fig. 5). Zircon grains in the basalt are rare and have short-prismatic to long-prismatic shapes, with lengths between 50 and 100 μm and length/width ratios of 1:1 to 2:1 (Fig. 5). They show broad zoning or/are homogenous (unzoned) and have Th and U contents ranging from 299 to 2863 ppm and 270 to 1598 ppm, respectively, with Th/U ratios of 0.98–1.79. CL images of zircon grains from the hornblende gabbro and gabbroic cumulate show rounded to long-prismatic shapes, with lengths between 100 and 300 μm and

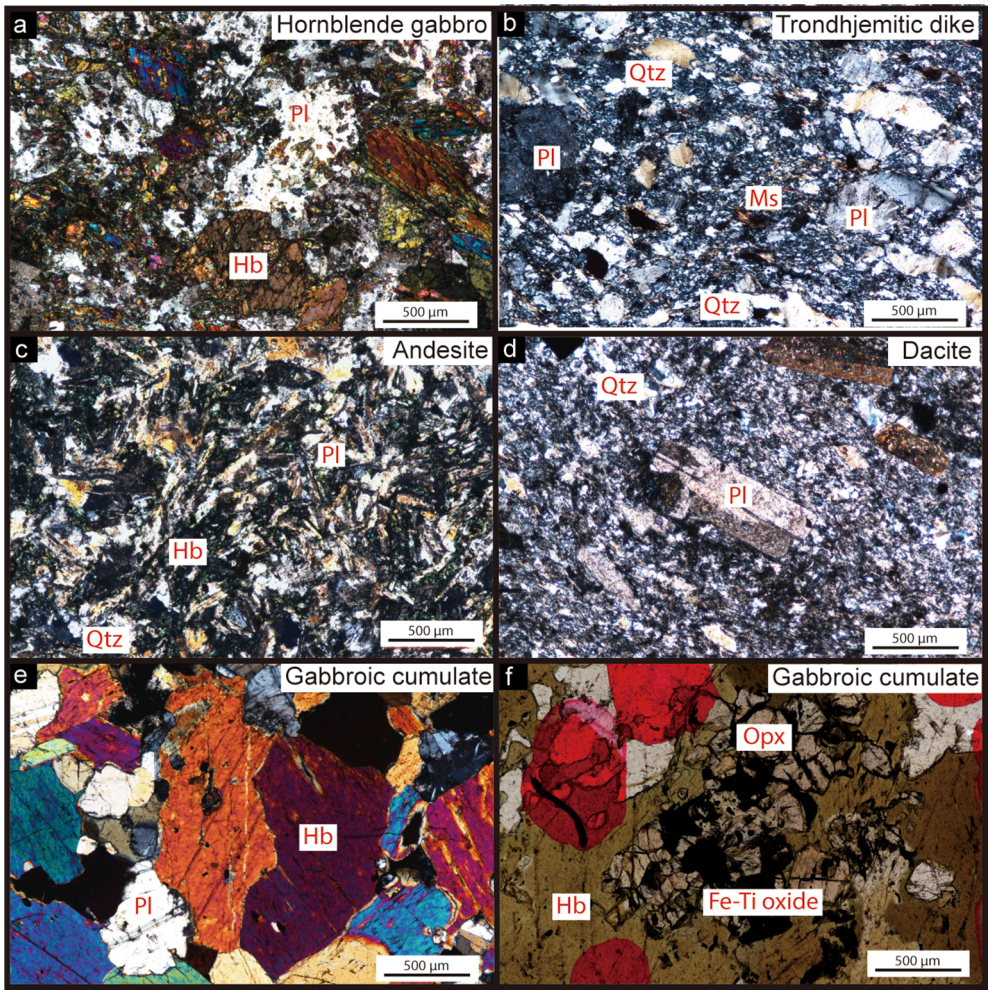

Fig. 4. Photomicrographs of the magmatic rocks in the Tachileik area showing (a) hornblende gabbro containing plagioclase and hornblende; (b) trondhjemitic dike containing quartz, plagioclase, muscovite; (c) andesite containing hornblende, plagioclase and quartz; (d) dacite containing plagioclase and quartz; (e and f) gabbroic cumulate containing hornblende, plagioclase, orthopyroxene, and Fe-Ti oxide. Mineral abbreviations: Opx, orthopyroxene; Hb, hornblende; Pl, plagioclase; Qtz, quartz; Ms, muscovite.

length/width ratios of 1:1 to 4:1, and display broad, sector, and oscillatory zoning (Fig. 5). They exhibit a wide range of Th (8–752 ppm) and U (28–1117 ppm) contents, with Th/U ratios of 0.10–1.18. Zircon grains from the andesite and dacite display broad zoning and oscillatory zoning and have short-prismatic to long-prismatic shapes, with lengths between 50 and 100 μm and length/width ratios of 1:1 to 4:1. They have low Th and U contents ranging from 36 to 428 ppm and 48 to 1057 ppm, respectively, with Th/U ratios of 0.17–1.76. Zircon grains from the trondhjemitic dike have rounded to long-prismatic shapes, with lengths between 50 and 100 μm and length/width ratios of 1:1 to 3:1 and display mainly oscillatory zoning with some of them showing metamict features with pores and resorption cores (Fig. 5). They have a wide range of Th (60–2836 ppm) and U (44–4724 ppm) contents, and variable Th/U ratios of 0.10–2.67. The zircons with metamict textures show elevated Hf with increasing U content (Fig. S1), which should be related to metamictization (Rubatto, 2002; Yang et al., 2014). Therefore, most zircons are of magmatic origin and some underwent deuteric alteration (Corfu et al., 2003; Rubatto, 2002).

A total of ten zircon spots are analyzed for U-Pb dating of basalt sample 19MY31. All analyses are plotted on the concordia curve, yielding a weighted mean $^{206}Pb/^{238}U$ age of 357 ± 2 Ma (MSWD = 1.0), which represents the crystallization age of this sample (Fig. 6a). Seven Lu-Hf isotopic analyses give $\varepsilon_{Hf}(t)$ values of −1.6 to + 3.8 (Fig. 7a).

Twenty spots are analyzed for hornblende gabbro sample 19MY29, and all analyses are plotted on the concordia curve, yielding a weighted mean $^{206}Pb/^{238}U$ age of 360 ± 3 Ma (MSWD = 0.23), which represents the magmatic crystallization age (Fig. 6b). Fifteen analyses of Hf-O isotope compositions give $\varepsilon_{Hf}(t)$ values of + 1.6 to + 5.5 and $\delta^{18}O_{VSMOW}$ values of 5.2‰ to 5.7‰ (average = 5.5 ± 0.3 ‰ (2σ)) (Fig. 7a and b).

A total of forty spots are analyzed for trondhjemitic dike sample 19MY30, including 20 SIMS analyses and 20 LA-ICP-MS analyses, and thirty spots are analyzed for sample 19MY32. All these analyses obtained similar results. Both samples yield older apparent $^{206}Pb/^{238}U$ ages of 2591 ± 39 Ma (SIMS, 19MY30), 2061 ± 21 Ma (LA, 19MY30), 2031 ± 43 Ma (LA, 19MY32), and 606 ± 10 Ma (SIMS, 19MY30), which are interpreted to represent inherited zircons. These two samples obtain similar weighted $^{206}Pb/^{238}U$ ages of 357 ± 7 Ma (MSWD = 1.6) (SIMS, 19MY30) and 355 ± 4 Ma (MSWD = 0.94) (LA, 19MY32) (Fig. 6c-f). Only one LA-ICP-MS analysis of 19MY30 yield apparent $^{206}Pb/^{238}U$ ages of 360 ± 5 Ma. The remaining analyses of both samples yield ages from 334 Ma to 211 Ma. Twenty grains of 19MY30 and fifteen grains of 19MY32 are analyzed for Hf-O isotopes. The zircons with older ages have $\varepsilon_{Hf}(t)$ values of −13.0 to + 1.9, and $\delta^{18}O_{VSMOW}$ values of 5.8–7.0‰ (Fig. 7a and b). The zircons with weighted mean ages of 357 ± 7 Ma and 355 ± 4 Ma have $\varepsilon_{Hf}(t)$ values of −11.8 to + 6.7, and $\delta^{18}O_{VSMOW}$ values of 5.2–7.3‰ (Fig. 7a and b). The remaining zircons with younger ages have $\varepsilon_{Hf}(t)$ values of −19.0 to + 5.4, and $\delta^{18}O_{VSMOW}$ values of 4.9–9.8‰. These trondhjemitic dikes show a complex age spectrum, and their crystallization time is discussed below. The inherited zircons could be rich in crystallized rocks, if the melting temperature is too low to dissolve zircons in the source rocks (Miller et al., 2003). However, the Hf-O isotopic compositions of the youngest zircons are different from those of predominant 357–355 Ma zircons, which is most likely of the magma source. In addition, the Hf-O isotopic compositions of these youngest zircons are not compatible with their own whole-rock Sr-Nd

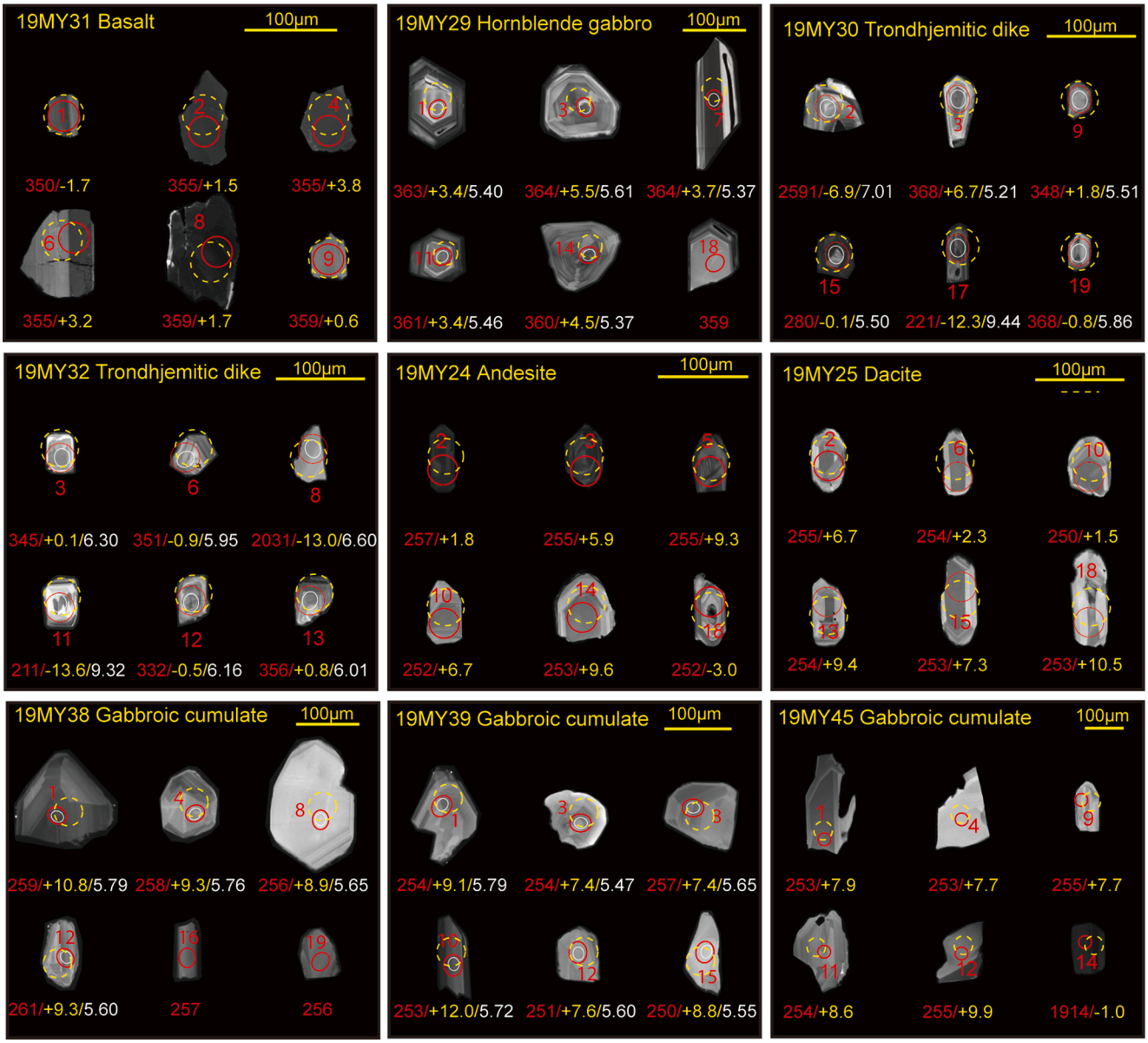

Fig. 5. Cathodoluminescence images of representative zircon grains from samples of basalt (19MY31), hornblende gabbro (19MY29), trondhjemitic dike (19MY30 and 19MY32), andesite (19MY24), dacite (19MY25), and gabbroic cumulate (19MY38, 19MY39 and 19MY45) showing their internal structures and analyzed locations. The red circles indicate zircon in situ U–Pb analyses with beam diameters of 32 μm for LA–ICP–MS (U–Pb) and 20 × 30 μm for SIMS (U–Pb). The yellow dashed circles indicate zircon in situ Lu–Hf isotope analyses with a beam diameter of 44 μm. The white circles indicate zircon in situ O isotope analyses with beam diameters of 15 × 20 μm. Apparent ages (in red), εHf(t) (in yellow), and $\delta^{18}O_{VSMOW}$ (in white) are also shown. Data are given in Supplementary Tables S2 and S3.

isotopic compositions (see next section). Because no ~ 350–280 Ma magmatic rocks in the study area, we consider that the zircons with ages of ~ 350–280 Ma are not inherited or captured. The predominant 357–355 Ma zircons show different textures, sizes, and chemical compositions (Th/U) from those nearby coeval mafic rocks, indicating that they are also not inherited or captured (Fig. S1). Combined with their relatively intact grains with clear internal textures (Fig. 5), we suggest that the 357 ± 7 Ma and 355 ± 4 Ma represent the crystallization ages. The younger ages are most likely formed by recrystallization and metamictization during later thermal events. Compared to those of 357–355 Ma zircons, more than half of young zircons have discordant ages. Although young concordant zircons show no positive correlation between U and Hf contents, indicating that they are not influenced by metamictization, a trend of decreasing Th/U ratios with decreasing ages is observed and some of them have very low Th/U ratios (Fig. S1). Near-concordant U-Pb zircon ages could be spanning hundreds of million years due to partial recrystallization if the lattice of zircon is not fully reconstructed (Halpin et al., 2012). The partial recrystallization most likely occurs in a solid state with or without a fluid phase (Geisler et al., 2007; Hoskin and Black, 2000). These young ages are mainly coeval to regional tectono-magmatic events, and this could be the reason for partial recrystallization. The partial recrystallization will not modify the Hf isotopic compositions (Halpin et al., 2012), as observed in our samples (Fig. 7c). Therefore, we re-calculate $\varepsilon_{Hf}(t)$ values for zircons with younger ages using the crystallization age of the sample. The large range of $\varepsilon_{Hf}(t)$ and $\delta^{18}O_{VSMOW}$ values may reflect supracrustal assimilation during magma ascent and emplacement.

A total of twenty spots are analyzed for andesite sample 19MY24. Eight analyses (#5, #8–9, #13, #15–17, #20) fall below the concordia curve, indicating possible Pb loss. Four analyses yielded older apparent $^{206}Pb/^{238}U$ ages of 1441 ± 14 Ma, 1425 ± 12 Ma, 1128 ± 10 Ma, and 386 ± 4 Ma, indicating that they may be captured/inherited zircon

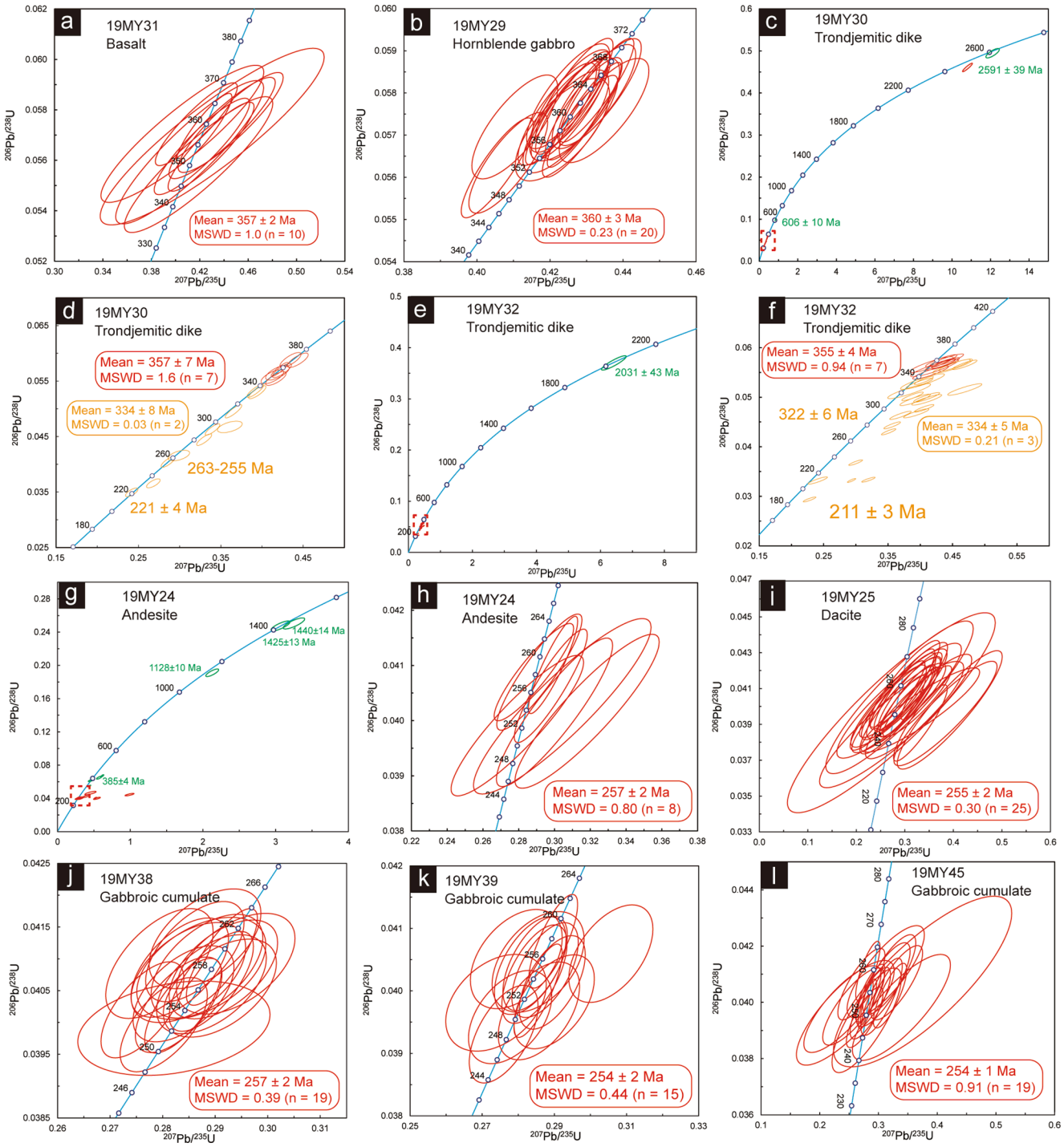

Fig. 6. U–Pb isotopic data for representative samples from the magmatic rocks in the Tachileik area. (a) basalt (19MY31); (b) hornblende gabbro (19MY29); (c-d) trondhjemitic dike (19MY30); (e-f) trondhjemitic dike (19MY32); (g-h) andesite (19MY24); (i) dacite (19MY25); (j-l) gabbroic cumulate (19MY38, 19MY39 and 19MY45). Datapoint error ellipses are 2σ.

(Fig. 6g and h). The remaining eight analyses yield a weighted mean $^{206}Pb/^{238}U$ age of 257 ± 2 Ma (MSWD = 0.80) (Fig. 6h). Ten zircon grains are selected for Hf isotopic analysis. The captured zircons (1441 Ma, 1425 Ma, 386 Ma, and 344 Ma) give $\varepsilon_{Hf}(t)$ values of + 14.2, +1.0, −10.3, and −11.7, respectively (Fig. 7a and b). The remaining six analyses are corrected to the magmatic crystallization age of 257 Ma, and yield $\varepsilon_{Hf}(t)$ values of −2.9 to + 9.7 (Fig. 7a and b).

Twenty-five spots are analyzed for dacite sample 19MY25, and all analyses yield a weighted mean $^{206}Pb/^{238}U$ age of 255 ± 2 Ma (MSWD = 0.30) (Fig. 6i). Twenty of them are selected for Hf isotopic analysis, yielding $\varepsilon_{Hf}(t)$ values of + 1.6 to + 10.8 (Fig. 7a).

A total of nineteen spots, sixteen spots, and twenty spots are analyzed for gabbroic cumulate samples 19MY38, 19MY39 and 19MY45, respectively (Fig. 6j-l). All analyses are plotted on the concordia curve, and two analyses yield older apparent $^{206}Pb/^{238}U$ age of 1846 ± 14 Ma (19MY39) and 1909 ± 12 Ma (19MY45). These three samples have a similar weighted mean $^{206}Pb/^{238}U$ age of 257 ± 2 Ma (MSWD = 0.39, 19MY38), 254 ± 2 Ma (MSWD = 0.44, 19MY39), and 254 ± 1 Ma (MSWD = 0.91, 19MY45) (Fig. 6j-l). Fifteen zircons of sample 19MY38 are selected for Hf-O isotope analyses, yielding $\varepsilon_{Hf}(t)$ values of + 8.3 to

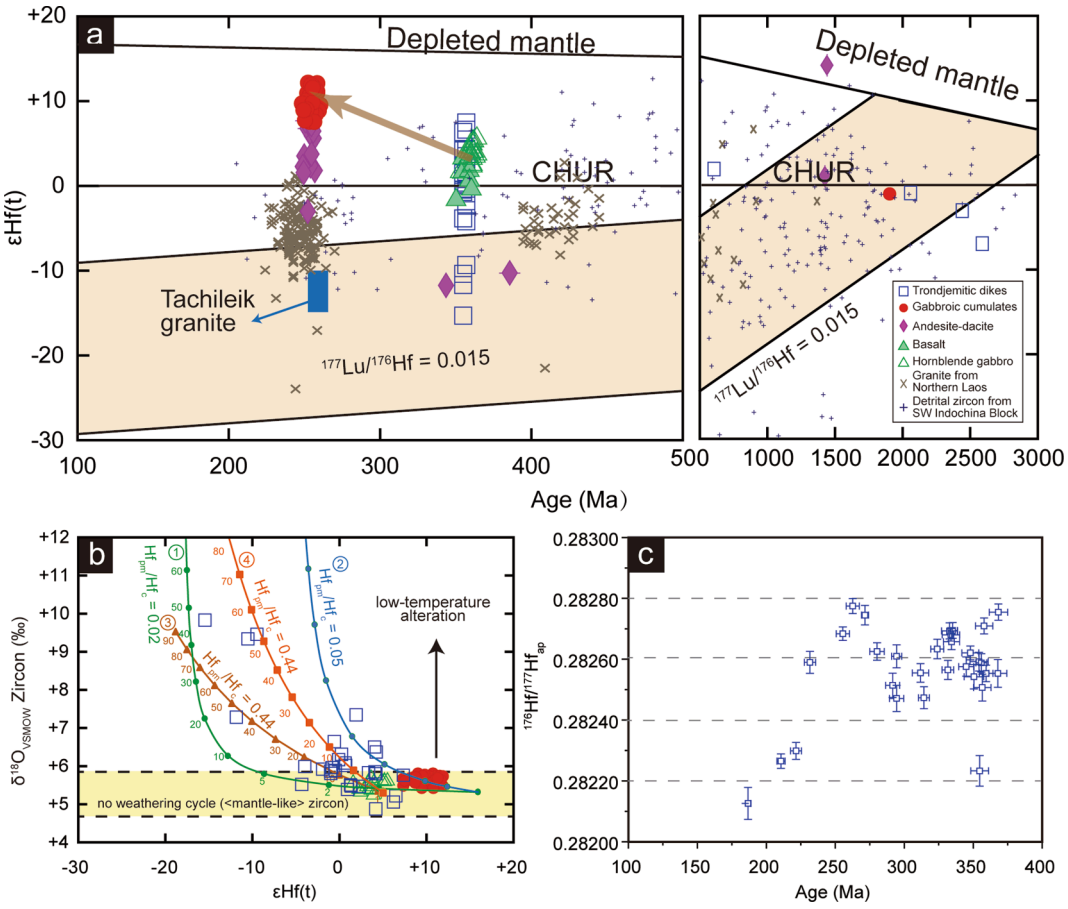

Fig. 7. Zircon Hf-O isotopic characteristics for magmatic rocks in the Tachileik area. (a) Plots of zircon $\varepsilon_{Hf}(t)$ values versus crystallization ages. The detrital zircon data of SW Indochina Block is from Arboit et al. (2016). The granites from Northern Laos are based on Wang et al. (2016a). The Tachileik granite data is after Gardiner et al. (2016). Reference lines representing meteoritic Hf evolution (CHUR) and that of the depleted mantle (DM) are from Blichert-Toft and Albarède (1997) and Griffin et al. (2000), respectively. (b) Zircon $\delta^{18}O$ versus $\varepsilon_{Hf}(t)$ of this study, showing calculated curves corresponding to magma evolution by simple mixing and crustal assimilation-fractional crystallization (AFC). The ratio of Hf concentrations in the parental magma (pm) and crustal (c) end-members (Hf_{pm}/Hf_c) is indicated. The $\delta^{18}O$ for the mantle is from Valley et al. (1998). The detailed parameters used in the modeling are listed in Supplementary Table S4. (c) Plots of apparent $^{176}Hf/^{177}Hf$ ratios versus ages of zircons from trondhjemitic dikes. Datapoint errors are 1σ.

+ 11.9 and $\delta^{18}O_{VSMOW}$ values of 5.3‰ to 5.6‰, with an average of 5.4 ± 0.1 ‰ (2σ) (Fig. 7a and b). Fifteen of zircons from sample 19MY39 are analyzed for Hf-O isotopes and yield $\varepsilon_{Hf}(t)$ values of + 7.4 to + 12.0 and $\delta^{18}O_{VSMOW}$ values of 5.4‰ to 5.8‰, with an average of 5.7 ± 0.2 ‰ (2σ) (Fig. 7a and b). Fourteen zircons from sample 19MY45 are selected for Hf isotopic analysis. The older zircon (1912 Ma) gives a $\varepsilon_{Hf}(t)$ value of −1.0. The remaining thirteen analyses, corrected to the magmatic crystallization age of 257 Ma, give $\varepsilon_{Hf}(t)$ values of + 7.7 to + 10.8 (Fig. 7a and b).

5.2. *Whole-rock geochemistry*

The major and trace element compositions of the magmatic rocks from the Tachileik area, eastern Myanmar are given in Supplementary Table S5. The gabbroic cumulate and trondhjemitic dike samples have low LOI values of < 2 wt% and show no or minor secondary minerals. The deuteric alteration usually results in the non-charge-and-radius-controlled (non-CHARAC) behavior of whole-rock REE (Yang et al., 2014), which is not observed for trondhjemitic dikes. Hence, we suggest that their whole-rock composition could be used for petrogenetic discussion. The hornblende gabbro and volcanic rocks (basalt, andesite and dacite) have slightly higher LOI (2.01–3.99 wt%) which is caused by weak to moderate alteration. Their microscopic texture features also indicate that they experienced post-magmatic alteration (Fig. 4). The concentrations of mobile elements (e.g., Ca, Na, K, Rb, Sr, Ba) are usually modified during alteration (Hastie et al., 2007). Therefore, mobile elements of hornblende gabbro and volcanic rocks are not suitable for rock classification and petrogenetic discussion.

5.2.1. *Basalt and hornblende gabbro*

The hornblende gabbro and basalt have low SiO_2 contents (47.6–51.9 wt%) and belong to the medium-K calc-alkaline series in the Th vs. Co diagram and the high-K calc-alkaline series in the K_2O vs. SiO_2 diagram (Fig. 8a-d). They have high TiO_2 (1.15–1.40 wt%) and TFe_2O_3 (total Fe_2O_3; 10.8–12.4 wt%) contents, and moderate CaO (4.21–5.75 wt%) contents (Fig. 8g-i). The basalt has higher MgO (9.89 wt%), Mg# (61), Cr (405 ppm) and Ni (152 ppm) values than the hornblende gabbro (5.06 wt%, 48, 3.55 ppm, 13.8 ppm). Chondrite-normalized REE patterns of the hornblende gabbro and basalt show slightly fractionated patterns with moderate (La/Yb) ratios of 3.40–3.90 and moderate to weak negative Eu anomalies (δEu = 0.6–0.9) (δEu = $Eu_N/SQRT(Sm_N*Gd_N)$; subscript N represents the chondrite-normalized value; Sun and McDonough, 1989) (Fig. 9a). These samples are enriched in large ion lithophile elements (LILE), such as Rb, Ba and Th, and are depleted in Nb, Ta and Zr in the primitive mantle-normalized multi-element diagram (Fig. 9b).

5.2.2. *Trondhjemitic dike*

The trondhjemitic dikes have extremely high SiO_2 contents (78.8–79.4 wt%) and belong to the medium-K calc-alkaline series in the

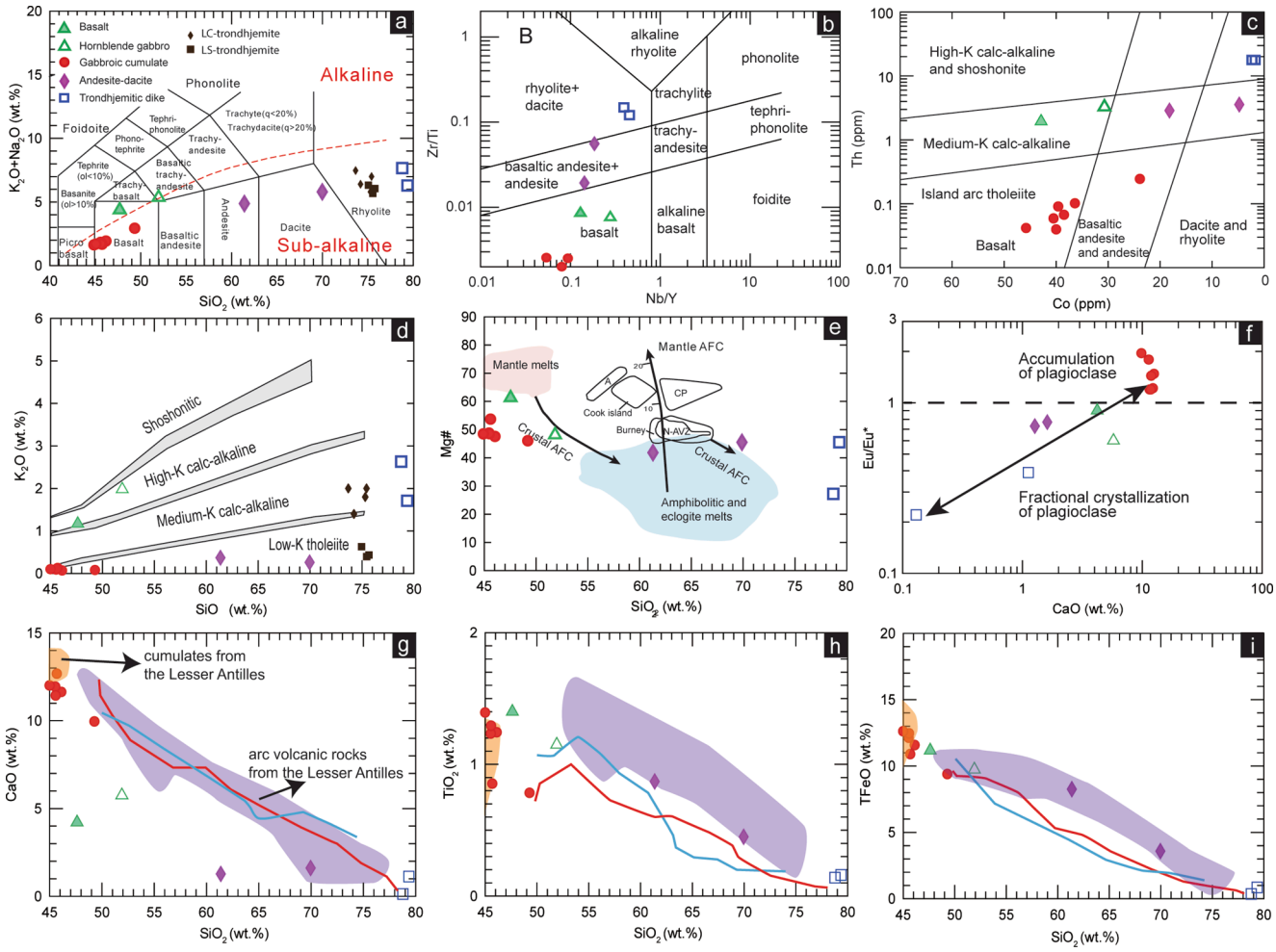

Fig. 8. Petrochemical classification of samples from the Tachileik area and their geochemical characteristics. (a) Total alkalis versus silica diagram (TAS, after Bas et al., 1986). (b) Zr/Ti versus Nb/Y diagram (after Pearce and Norry, 1979). (c) Th versus Co diagram (after Hastie et al., 2007). (d) K_2O versus SiO_2 diagram (after Rollinson, 1993). (e) Mg# versus SiO_2 diagram (modified after Stern and Kilian, 1996). The field for pure crustal partial melts obtained in experimental studies by dehydration melting of amphibolitic rocks and eclogites (Rapp et al., 1999; Rapp and Watson, 1995; Sisson et al., 2005; Smithies, 2000). (f) Eu/Eu* versus CaO diagram. Data of low-Ca trondhjemite is from Fiannacca et al. (2020). Data of Longmuco-Shuanghu trondhjemite is from Dan et al. (2018). Abbreviations: LC-trondhjemite, Low-Ca trondhjemite. LS-trondhjemite, Longmuco-Shuanghu trondhjemite. (g) CaO versus SiO_2 diagram. (h) TiO_2 versus SiO_2 diagram. (i) TFe_2O_3 versus SiO_2 diagram. Red and blue lines represent experimental liquid lines. Experimental liquid lines of descent are after Nandedkar et al. (2014) (red line) and Kawamoto (1996) (blue line). Data of arc volcanic rocks and cumulates from the Lesser Antilles are from Cooper et al. (2016, 2019).

K_2O vs. SiO_2 diagram and the high-K calc-alkaline in the Th vs. Co diagram (Fig. 8a-d). They have low TiO_2 (0.14–0.16 wt%), MgO (0.08–0.40 wt%), and CaO (0.13–1.12 wt%) contents, and high Na_2O (4.53–4.99 wt%) and Th (22.2–22.4 ppm) contents with metaluminous to peraluminous characteristics (A/CNK = 0.9–1.09; molar $Al_2O_3/(CaO + Na_2O + K_2O)$) (Fig. 9g-i). In the chondrite-normalized REE diagram, these trondhjemitic dikes have fractionated LREE/HREE patterns with (La/Yb) ratios of 2.36–4.97 and strongly negative Eu anomalies (δEu = 0.22–0.39) (Fig. 9c). These samples have high concentrations of LILE, such as Rb, Ba and Th, and show negative Nb-Ta anomalies and strong negative Sr, P and Ti anomalies in the primitive mantle-normalized multi-element diagram (Fig. 9d).

5.2.3. Andesite and dacite

The andesite and dacite have moderate SiO_2 contents (61.4–70.0 wt %) and are plotted in the medium-K calc-alkaline region in the Th vs. Co diagram and the low-K calc-alkaline region in the K_2O vs. SiO_2 diagram (Fig. 8a-d). They are peraluminous (A/CNK = 1.17–1.58) due to their low CaO (1.27–1.61 wt%) and K_2O (0.26–0.37 wt%) contents. They also exhibit low Rb (4.72–6.70 ppm), Ba (34.2–59.4 ppm) and Sr (102–106 ppm) contents. They show moderate MgO (1.68–3.33 wt%), Al_2O_3 (14.3–15.8 wt%), TiO_2 (0.45–0.87 wt%) and TFe_2O_3 (3.98–9.17 wt%) contents (Fig. 8). These samples are slightly enriched in light rare-earth elements (LREE) [$(La/Yb)_N$ = 2.16–2.85], with negative Eu anomalies (δEu = 0.7–0.8) in the chondrite-normalized REE diagram (Fig. 9e). They show enrichment in Th but are depleted in Rb, Ba, Sr and high field strength elements (HFSE) (e.g., Nb, Ta, and Ti) in the primitive mantle-normalized multi-element diagram (Fig. 9f).

5.2.4. Gabbroic cumulate

The gabbroic cumulate samples have low SiO_2 contents (44.9–49.3 wt%) and are plotted in the low-K tholeiite region in the Th vs. Co and K_2O vs. SiO_2 diagrams (Fig. 8a-d). They are characterized by low K_2O (0.06–0.12 wt%), Rb (0.94–1.96 wt%) and Th (0.04–0.24 wt%) contents and high MgO (4.45–8.38 wt%), CaO (9.93–12.65 wt%), TiO_2 (0.78–1.39 wt%), Al_2O_3 (16.7–21.5 wt%), TFe_2O_3 (10.4–14.0 wt%), Cr (22–116 ppm), and V (177–477 ppm) contents (Fig. 8). These gabbroic cumulates have mainly flat REE patterns ($(La/Yb)_N$ = 0.81–1.18, except for sample 19MY40) and positive Eu anomalies (δEu = 1.19–1.94) (Fig. 9e). These samples show no negative Nb-Ta anomalies and are depleted in Rb, Th and Zr, but show positive Ba, Sr and Ti anomalies in the primitive mantle-normalized multi-element diagram (Fig. 9f).

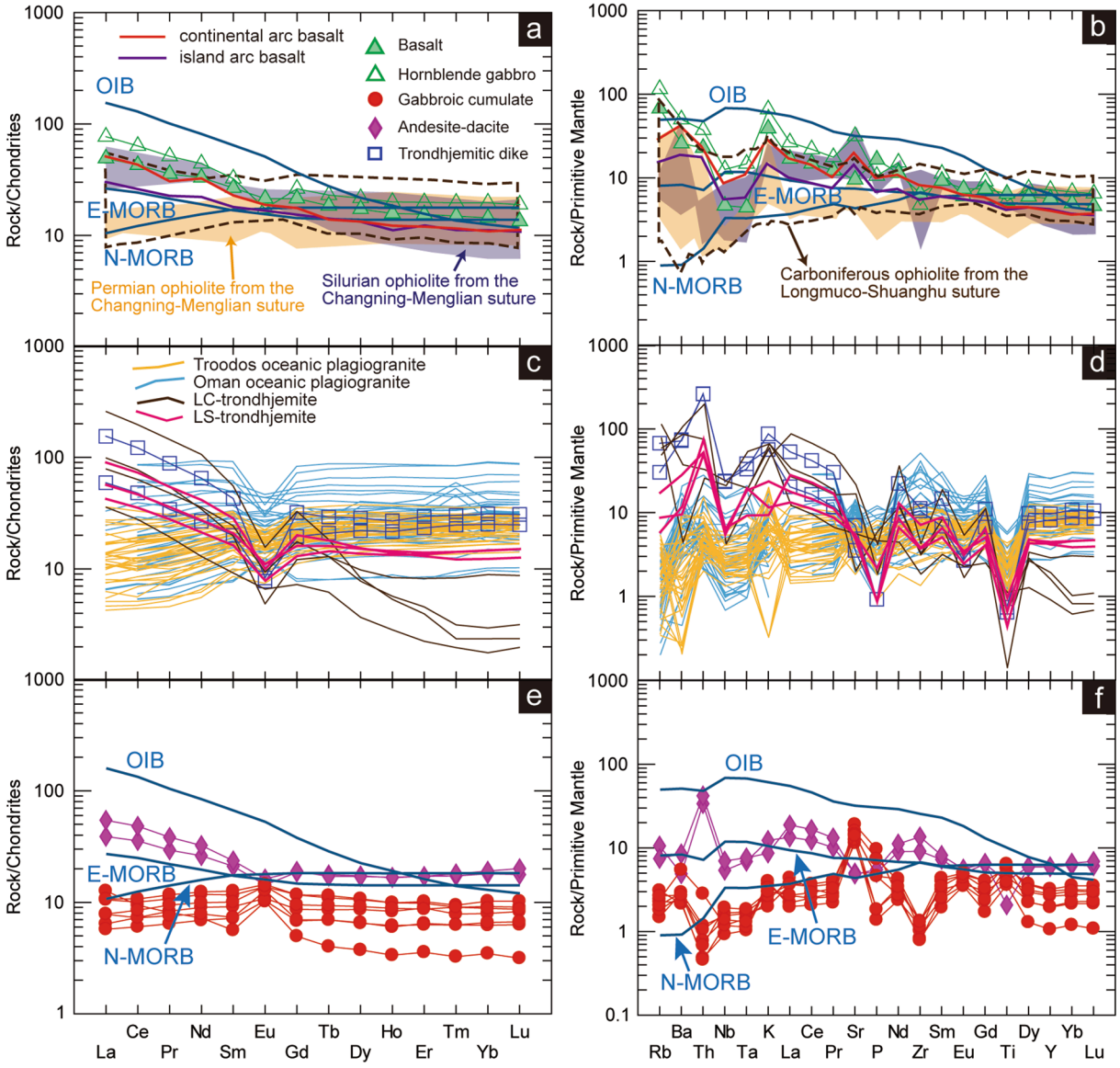

Fig. 9. Chondrite-normalized REE patterns and primitive mantle-normalized multi-element patterns for samples from (a) and (b) basalt and hornblende gabbro; (c) and (d) trondhjemitic dike; (e) and (f) andesite-dacite and gabbroic cumulate. Normalization values and data of N-MORB, E-MORB and OIB are from Sun and McDonough (1989). Data of continental arc basalt and island arc basalt are from Kelemen et al. (2003). Data of Troodos oceanic plagiogranite are from Freund et al. (2014) and Marien et al. (2019). Data of Oman oceanic plagiogranite are from Rollinson (2009) and Haase et al. (2016).

5.3. *Whole-rock Sr-Nd isotopes*

Whole-rock Sr-Nd isotope composition data for the magmatic rocks in the Tachileik area, eastern Myanmar are given in Supplementary Table S6. The initial $^{87}Sr/^{86}Sr$ ratios and $\varepsilon_{Nd}(t)$ of magmatic rocks are calculated on the basis of their zircon U-Pb ages for the basalt (t = 360 Ma), hornblende gabbro (t = 360 Ma), trondhjemitic dike (t = 360 Ma), andesite (t = 255 Ma), and gabbroic cumulate (t = 255 Ma). The basalt has a $(^{87}Sr/^{86}Sr)_i$ value of 0.7033 and a $\varepsilon_{Nd}(t)$ value of + 2.1. Compared to the basalt, the coeval hornblende gabbro and trondhjemitic dike have more enriched Sr-Nd isotopic compositions with $(^{87}Sr/^{86}Sr)_i$ values of 0.7046 and 0.7047 and $\varepsilon_{Nd}(t)$ values of −0.2 and −0.6, respectively. The gabbroic cumulate has $(^{87}Sr/^{86}Sr)_i$ values of 0.7043 to 0.7045 and $\varepsilon_{Nd}(t)$ values of + 2.9 to + 3.3. In comparison to the gabbroic cumulate, the coeval andesite has a more enriched Sr-Nd isotopic composition with a $(^{87}Sr/^{86}Sr)_i$ value of 0.7050 and a $\varepsilon_{Nd}(t)$ value of + 1.0. In general, they are plotted within the mantle array in the Sr-Nd isotopic diagram (Fig. 10a). In the Nd-Hf isotopic diagram, they are plotted slightly above the MORB-OIB array, except for the basalt sample which falls below the array (Fig. 10b).

5.4. *Mineral chemistry*

Representative major element compositions of orthopyroxene, feldspar and amphibole from the magmatic rocks in the Tachileik area, eastern Myanmar are reported in Supplementary Table S8. The representative photos of selected minerals are shown in Fig. S2.

5.4.1. *Orthopyroxene*

Orthopyroxene from the gabbroic cumulates are characterized by low MgO (14.63–19.03 wt%) and Mg# (44–55) values, and high TFeO (total FeO, 27.87–32.76 wt%) contents. Sample 19MY40 shows slightly higher Mg# values than 19MY41 and 19MY42. Collectively, the orthopyroxenes are classified as clinoenstatite and clinoferrosilite ($Wo_{1-2}En_{49-54}Fs_{44-49}$ (19MY40), $Wo_{1-2}En_{44-50}Fs_{49-55}$ (19MY41), $Wo_{1-2}En_{45-56}Fs_{53-54}$ (19MY42)) (Wo, wollastonite; En enstatite; Fs, ferrosillite)

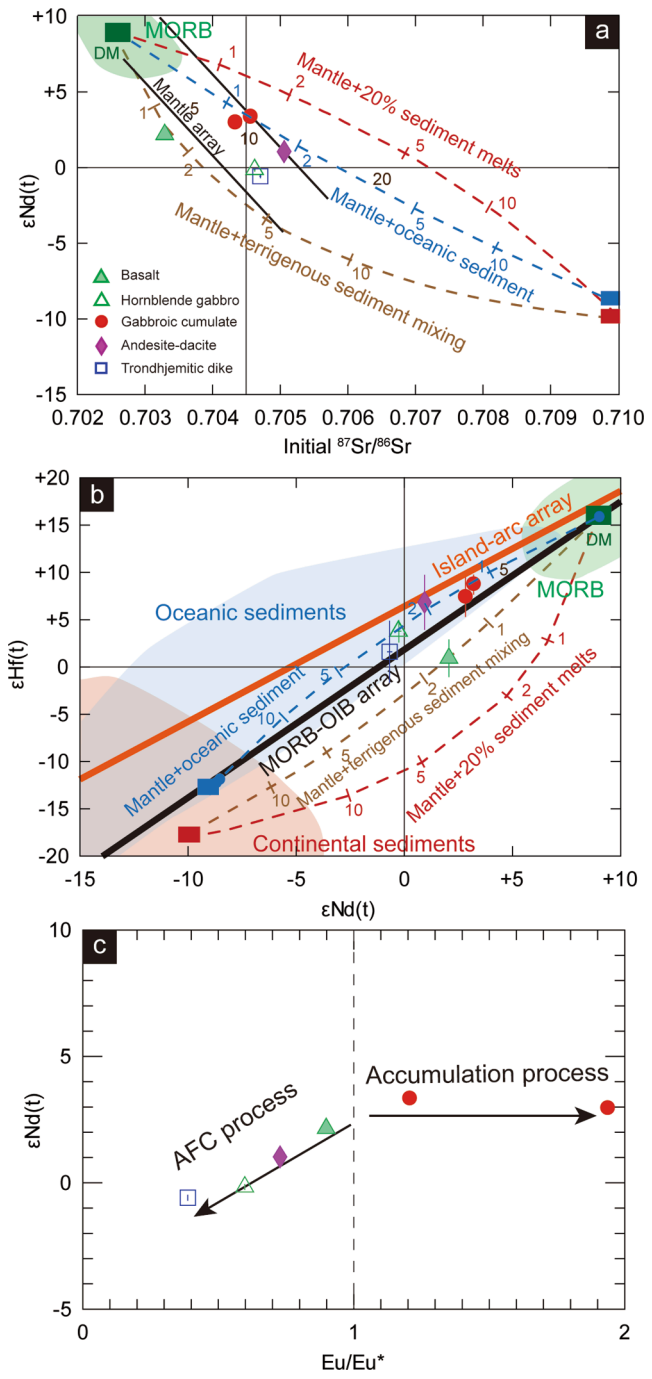

Fig. 10. Sr-Nd-Hf isotopic features of magmatic rocks from the Tachileik area. (a) $\varepsilon_{Nd}(t)$ versus initial $^{87}Sr/^{86}Sr$ diagram. (b) $\varepsilon_{Hf}(t)$ versus $\varepsilon_{Nd}(t)$ diagram. (c) $\varepsilon_{Nd}(t)$ versus Eu/Eu* diagram. Data of DM (depleted mantle) is from Salters and Stracke (2004). Data of MORB are based on Zindler and Hart (1986) and Chauvel et al. (2009). Data of oceanic sediments, Fe-Mn crust, and continental sediments are from Chauvel et al. (2008, 2014). MORB-OIB array and island-arc array are after Chauvel et al. (2009). Modeling parameters are listed in Supplementary Table S7.

(Fig. 11a).

5.4.2. Feldspar

In the gabbroic cumulates, feldspars are all labradorite and bytownite (Fig. 11b). Plagioclase from samples 19MY38 and 19MY39 has high An (anorthite) values (85–89) and plagioclase from sample 19MY40 has a wide range of An values (52–75). The plagioclases from the remaining gabbroic cumulates show consistent ranges of An values (73–90) (Fig. 11c). The plagioclases from the hornblende gabbro, andesite and dacite are mainly albite (An = 0–11) (Fig. 11b), reflecting secondary albitization of these samples. The feldspars in the trondhjemitic dikes include sanidine and albite (An = 0–2).

5.4.3. Amphibole

Amphibole from the gabbroic cumulate and hornblende gabbro are all calcic amphibole based on the classification of Hawthorne et al. (2012). Specific names of these calcic amphiboles according to this nomenclature show that these amphiboles are magnesiohornblende and tschermakite (Fig. 11d). Amphiboles from gabbroic cumulates show medium Mg# values (42–60), except for sample 19MY38, which has relatively high Mg# values (64–69) (Fig. 11c). The amphiboles from the hornblende gabbro also show medium Mg# values of 58–64 (Fig. 11c). The plagioclase-amphibole thermobarometer of Holland and Blundy (1994) was applied to unaltered plagioclase-amphibole pairs interpreted to have formed in equilibrium based on textural relationships. The calculated temperatures of gabbroic cumulates range from 781 to 944 °C (average 853 °C ± 38 (std), T_{HB}, temperature according to Holland and Blundy (1994)), 786 to 890 °C (average 817 °C ± 21 (std), T_R, temperature according to Ridolfi et al. (2010)), and 706 to 863 °C (average 792 °C ± 26 (std), T_{RR}, temperature according to Ridolfi and Renzulli (2012)), and calculated pressures range from 1.0 to 4.1 kbar (average 1.7 kbar ± 0.4 (std), P_R, pressure according to Ridolfi et al. (2010)) and 1.1 to 3.9 kbar (average 1.7 kbar ± 0.4 (std), P_{RR}, pressure according to Ridolfi and Renzulli (2012)) (Fig. 9e). The calculated SiO_2 contents of equilibrium melts based on the amphibole from gabbroic cumulates are between 66.7 wt% and 78.0 wt% (Fig. 11f). The calculated temperatures of hornblende gabbro ranges from 746 to 809 °C (average 781 °C ± 19 (std), T_R), and 704 to 777 °C (average 746 °C ± 28 (std), T_{RR}), and calculated pressures range from 0.7 to 1.2 kbar (average 1.0 kbar ± 0.2 (std), P_R) and 0.7 to 1.3 kbar (average 1.0 kbar ± 0.3 (std), P_{RR}) (Fig. 11e).

6. Discussion

6.1. Petrogenesis of magmatic rocks in eastern Myanmar

6.1.1. Basalt and hornblende gabbro

Field relationships, whole-rock geochemistry, and isotopic compositions suggest that the basalt and hornblende gabbro have a close genetic relationship and they may share a common magma source (Figs. 7-10). Their low SiO_2 contents and depleted isotopic composition of Sr-Nd-Hf-O indicate that they must be derived from a mantle source. Compared to the basalt, the hornblende gabbro shows an elevated initial $^{87}Sr/^{86}Sr$ and lower Mg#, Eu/Eu* and $\varepsilon_{Nd}(t)$ (Fig. 8f and 10c), indicating that the hornblende gabbro experienced assimilation and fractional crystallization during magma emplacement. Therefore, the basalt composition may be closer to the original composition of the mantle-derived melt.

According to the Sr-Nd isotope composition, the basalt was derived from a depleted mantle source (Fig. 10a). The trace-element pattern of the basalt shows similarity to arc basalts with enrichment of LREE and depletion of Nb-Ta (Fig. 9a and b), indicating that the mantle source was metasomatized by subduction-related processes. Traditional models suggested that the mantle wedge can be metasomatized by slab-derived fluids or slab-derived melts (Turner and Langmuir, 2015; Wu et al., 2020a). Recently, a mélange diapir model was proposed in which subducted sediments, altered oceanic crust, and hydrated mantle physically mixed to form mélange rocks and that mixture involved in the partial melt to form an arc magma (Marschall and Schumacher, 2012; Nielsen and Marschall, 2017). Therefore, there are three potential enrichment end members including slab-derived fluids, slab-derived melts (sediment melts and mafic oceanic crust melts), and slab-derived mélange. The enriched Sr-Nd-Hf isotopic composition of the Tachileik basalt is not consistent with pure slab-derived fluids (Fig. 10a and b). The basalt

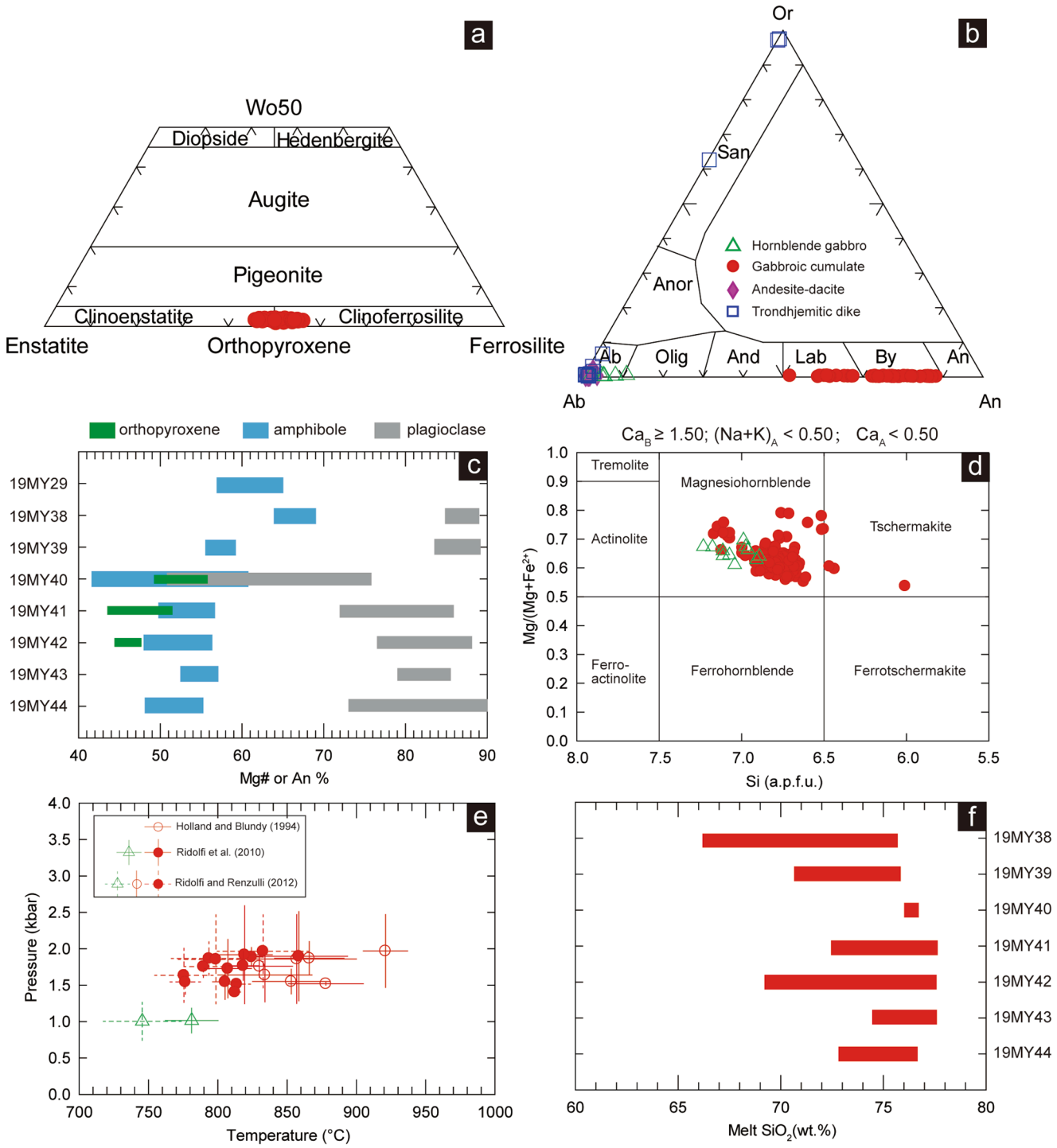

Fig. 11. Mineral composition of magmatic rocks from the Tachileik area. (a) Orthopyroxenes from the gabbroic cumulate plotted on the enstatite–ferrosilite–diopside–hedenbergite quadrilateral of Morimoto (1988). (b) Ab–Or–An diagram for feldspar. Or, potassium feldspar; San, Sanidine; Anor, anorthoclase; Ab, albite; Olig, oligoclase; And, andesine; Lab, labradorite; By, bytownite; An, anorthite. (c) Mg# or An % of orthopyroxene, hornblende, and plagioclase from hornblende gabbro and gabbroic cumulate. (d) Classification of amphibole according to the nomenclature of Hawthorne et al. (2012). (e) Calculated pressure and temperature based on hornblende and plagioclase from hornblende gabbro and gabbroic cumulate (Holland and Blundy, 1994; Ridolfi et al., 2010; Ridolfi and Renzulli, 2012). (f) Calculated SiO_2 of equilibrium melt based on hornblende from gabbroic cumulate (Ridolfi and Renzulli, 2012). The calculated results are listed in Supplementary Table S9.

exhibits decoupled Hf-Nd isotope ratios that are plotting below the MORB-OIB array (Fig. 10b), indicating that excess zircon is incorporated into the mantle wedge (Chauvel et al., 2014). Subducted sediments, especially terrigenous sediments which are enriched in Zr contents may be responsible for this enrichment.

To discriminate between potential enrichment sources (oceanic sediments, terrigenous sediments, sediment melts), we used isotopic mixing modeling to show different trajectories of enrichment by different sources (Fig. 10a and b). Oceanic sediments usually are plotted on or above the MORB-OIB array (Fig. 10b). Therefore, mixing between oceanic sediments and depleted mantle will be also plotted above the MORB-OIB array, which is contrary to the isotopic composition of the

Tachileik basalt (Fig. 10b). More enriched Hf isotopic composition than Nd isotopic composition of a mantle-derived melt could be achieved by the addition of terrigenous sediments or sediment-derived melts. In addition, distinct trends of these two different end-members could be observed in both Hf-Nd and Sr-Nd isotope diagrams (Fig. 10a and b). Collectively, our isotopic modeling results show that the addition of 1–2% terrigenous sediment could lead to the enrichment of the Sr-Nd-Hf isotopic composition of the depleted mantle. This small amount of sediment will not change the O isotope composition significantly (Fig. 7b). Furthermore, such a process indicates that sediment, rather than sediment-derived melt, is mixed with the mantle peridotite, which is consistent with the mélange diapir model (Marschall and Schumacher, 2012; Nielsen and Marschall, 2017). Except for the isotopic compositions, this model could also explain the trace element enrichments. According to our trace element modeling (Fig. 12a), the addition of 2% subducted sediments to the mantle wedge could increase the Th/Yb and the Nb/Yb ratios, resulting in a mixed source plotted above the mantle array in the Th/Yb vs. Nb/Yb diagram. Ten percent partial melting of spinel-garnet lherzolite could generate melt with similar compositions to the basalt in both Th/Yb vs. Nb/Yb and Sm/Yb vs. Sm diagrams (Fig. 12b). Therefore, we propose that the basalt in eastern Myanmar was formed by partial melting of mélange diapirs, and that the hornblende gabbro was formed by assimilation and fractional crystallization of the basaltic magma.

6.1.2. Trondhjemitic dike

Four petrogenetic mechanisms to explain the origin of trondhjemite have been proposed, which are (1) partial melting or fractional crystallization of MORB in the mid-oceanic ridge or fore-arc (Freund et al., 2014; Rollinson, 2009); (2) water-fluxed melting of metapelite or metagreywacke (Fiannacca et al., 2020); (3) high-pressure dehydration melting of basaltic rocks (Martin et al., 2005; Sun et al., 2020); and (4) low-pressure fractional crystallization of basaltic arc rocks (Dan et al., 2019).

A major subgroup of trondhjemite is oceanic plagiogranite, formed by partial melting or fractional crystallization of MORB in the mid-oceanic ridge or fore-arc, which can be found in the ophiolitic mélanges (Freund et al., 2014; Rollinson, 2009). However, our trondhjemitic dikes show geochemical features inconsistent with those of oceanic plagiogranite (Fig. 9c and d). The Tachileik trondhjemitic dikes display higher K_2O contents, and larger Nb/Y and Th/La ratios compared to oceanic plagiogranite (Fig. 8d and 12c-d), indicating that they have a different petrogenesis. In addition, zircon trace element compositions from the trondhjemitic dikes are plotted in the area of the continental arc-type zircon (Fig. 12e and f; Grimes et al., 2015). Therefore, the trondhjemitic dikes in eastern Myanmar are not part of an ophiolitic mélange.

Although some zircons from the trondhjemitic dikes show elevated $\delta^{18}O_{VSMOW}$ and enriched Hf isotopic features, most of the zircons display positive $\varepsilon_{Hf}(t)$ values and mantle-like $\delta^{18}O_{VSMOW}$ values (Fig. 7; Valley, 2003), indicating that their primary source is not metapelites/metagreywackes. This is also supported by their whole-rock Sr-Nd isotopic compositions, which are similar to the coeval hornblende gabbro (Fig. 10). The zircons with enriched $\delta^{18}O_{VSMOW}$ isotopic composition may be formed by assimilation of the supracrustal materials or low-temperature alteration (Valley, 2003). Partial melting of basaltic rocks at high pressure could produce trondhjemite, e.g., Archean trondhjemite (Martin et al., 2005). The most significant characteristic of this high-pressure trondhjemite is their high La/Yb and Sr/Y ratios, suggesting that their source region contains restitic garnet (Martin et al., 2005; Sun et al., 2020). Such characteristics were not observed in the trondhjemitic dikes in this study, and they show very low La/Yb and Sr/Y ratios with strongly negative Eu anomalies (Fig. 9c). Low La/Yb and Sr/Y ratios and negative Eu anomalies may be caused by partial melting and fractional crystallization at low-pressure conditions, where plagioclase is stable. This model has been proposed for the Longmuco-Shuanghu trondhjemite (Dan et al., 2019), which has a similar geochemical feature to our samples. The Tachileik trondhjemitic dike sample with higher CaO content shows lower Rb and LREE contents and higher Sr content, which is consistent with the fractional crystallization model. Therefore, we suggest that these trondhjemitic dikes were formed by fractional crystallization of melts derived from partial melting of basaltic rocks at a low-pressure condition.

There are two main reasons why we believe that the source of these trondhjemitic dikes is the coeval basaltic rocks. First, as discussed above, the isotopic compositions of the trondhjemitic dikes are similar to the coeval hornblende gabbro and the two igneous units have a close spatial distribution and similar formation ages. Second, these trondhjemitic dikes intruded into the hornblende gabbros and there is no coeval intermediate magma, suggesting that the trondhjemitic dikes are most likely formed by partial melting of the basaltic rocks, but not by fractionation of the basaltic melts. In conclusion, we suggest that these trondhjemitic dikes were formed by partial melting of hornblende gabbro and experienced fractional crystallization at a low-pressure condition.

6.1.3. Andesite, dacite and gabbroic cumulate

The formation ages of the Tachileik andesite and dacite and gabbroic cumulates are identical within error and may have a genetic relationship. The whole-rock geochemical compositions of the volcanic rocks and the gabbroic cumulates are comparable to volcanic arc rocks-cumulate rock pairs from arc settings and match experimental liquid lines of descent for arc rocks (Fig. 8; Cooper et al., 2016, 2019; Melekhova et al., 2015). The highest zircon $\varepsilon_{Hf}(t)$ value of these volcanic rocks is similar to that of the gabbroic cumulates (Fig. 7a), implying that their original sources could also be similar. The volcanic rocks are interpreted to be the melts after magma fractionation and the gabbroic cumulates are formed as the crystallized phase. The volcanic rocks show lower whole-rock $\varepsilon_{Nd}(t)$, MgO, Al_2O_3; TFeO, and TiO_2 contents, and Eu/Eu* ratios (Fig. 8f-i and 10c), compared to the gabbroic cumulates, indicating that these volcanic rocks may have formed by magma assimilation and fractional crystallization (AFC). The zircon Hf isotope generally could keep a record of such assimilation process showing a wide range of $\varepsilon_{Hf}(t)$ values instead of being unified like whole-rock Sr-Nd isotope (Amelin et al., 2000). The wide range of zircon $\varepsilon_{Hf}(t)$ values (Fig. 7a) indicates that these volcanic rocks could be formed by AFC of mantle-derived melts or magma mixing between the mantle-derived and crustal-derived melts. However, the low Mg#, and Cr, Co, and Ni contents of these volcanic rocks show no evidence of magma mixing. In addition, the old zircon ages found in these volcanic rocks proved that they have captured old crustal materials during the magma ascent. The wide range of zircon $\varepsilon_{Hf}(t)$ values of these volcanic rocks and their more enriched Sr-Nd isotopic features than that of the gabbroic cumulate were more likely caused by magma assimilation (Fig. 7a and 10c). Therefore, we suggest that the volcanic rocks are products of assimilation and fractional crystallization during magma ascent.

The gabbroic cumulates have the most depleted isotopic composition with Eu/Eu* ratios > 1, reflecting an accumulation process (Fig. 8). The mineral assemblage of the gabbroic cumulates (plagioclase, amphibole, orthopyroxene, and magnetite) is quite similar to shallow depth cumulates in volcanic arc systems (Cooper et al., 2016; Melekhova et al., 2015), indicating that these cumulates could be late crystallized phases. This is also supported by mineral chemistry. The gabbroic cumulates have low Mg# (<70) orthopyroxene and amphibole and low An content plagioclase (<90) (Fig. 11c). Based on the chemical composition of amphiboles from gabbroic cumulates, we calculated P-T conditions and SiO_2 contents of the equilibrated melt. The results show that they crystallized at a shallow depth in the crust (5–6 km), and that they equilibrated with a felsic magma which has similar SiO_2 contents to the volcanic rocks (Fig. 11e and f). These lines of evidence suggest that these cumulates formed in the late stages of magma fractionation. Therefore, we suggest that these gabbroic cumulates are products of the late

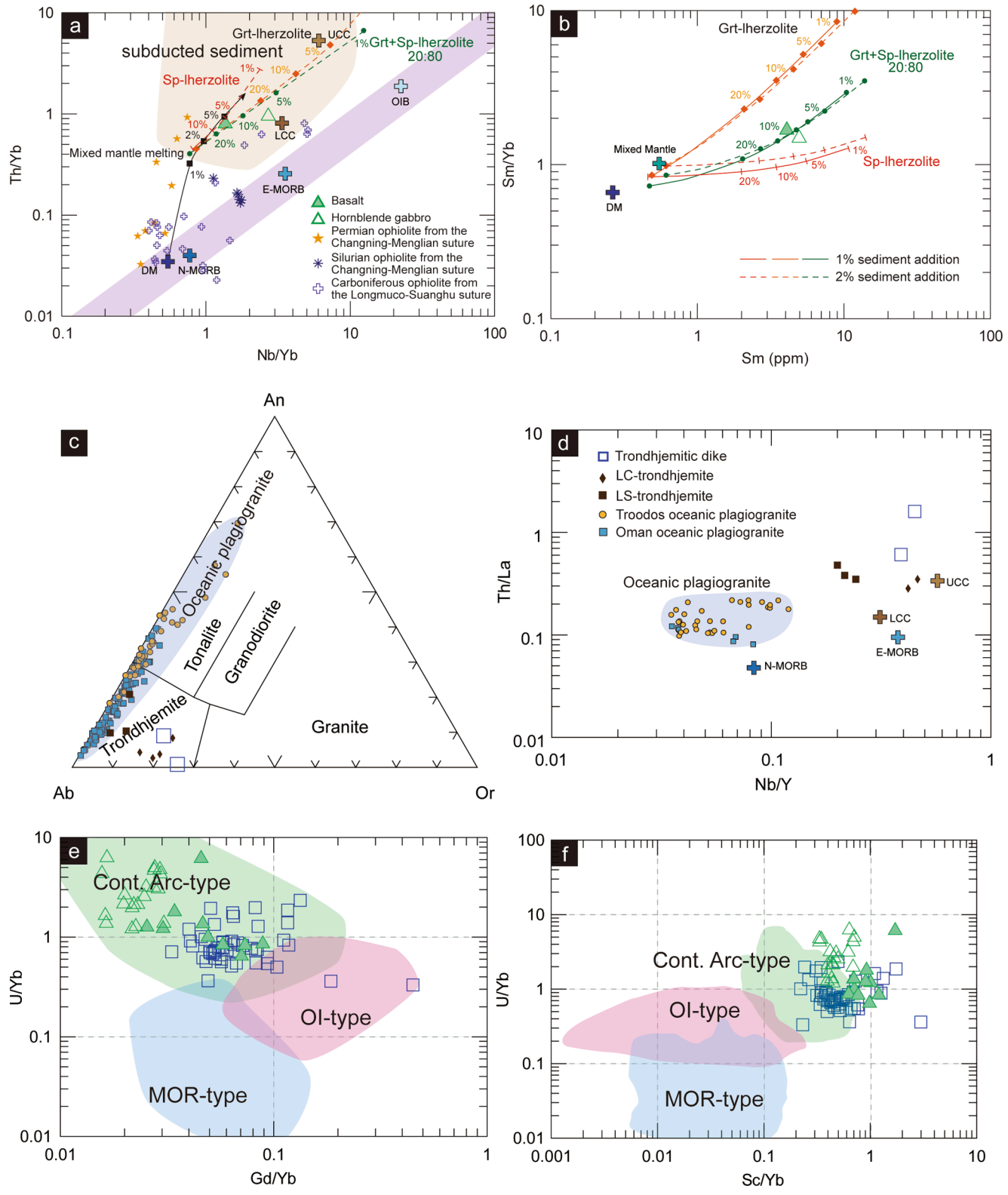

Fig. 12. Petrogenetic discrimination diagrams for magmatic rocks from the Tachileik area. (a) Th/Yb versus Nb/Yb diagram (after Pearce, 2008). (b) Sm/Yb versus Sm diagram. (c) An-Ab-Or diagram (Barker, 1979). Data of oceanic plagiogranite are from Rollinson (2009), Freund et al. (2014), Haase et al. (2016) and Marien et al. (2019). (d) Th/La versus Nb/Y diagram. Data of N-MORB and E-MORB are from Sun and McDonough (1989). Data of LCC (lower continental crust) and UCC (upper continental crust) are from Rudnick and Gao (2003). (e-f) U/Yb versus Gd/Yb diagram and U/Yb versus Sc/Yb diagram of zircon from trondhjemitic dike (after Grimes et al., 2015). Cont. Arc-type, continental arc zircon. MOR-type, mid-ocean ridge zircon; Ol-type, ocean island zircon. The modeling parameters are listed in Supplementary Table S10.

crystallized phase during magma ascent and the volcanic rocks are co-magmatic rocks that experienced magma assimilation and fractional crystallization.

The primary magma for these volcanic rocks and gabbroic cumulates could be derived from partial melting of the mantle source or from the melting of crustal rocks. In comparison with the Tachileik granite (Gardiner et al., 2016) and our previously discussed basaltic rocks, these rocks have more depleted isotopic features (Fig. 7a). This suggests that the primary magma is not derived from the continental crust of the Sukhothai arc. The Sr-Nd-Hf isotopic compositions of the gabbroic cumulates are plotted slightly above the mantle array (Fig. 10a and b), which we interpret to reflect enrichment by subducted oceanic sediments (Vervoort et al., 2011). We suggest that the more enriched isotopic compositions of volcanic rocks are related to the subsequent intracrustal assimilation and fractional crystallization (Fig. 7a and 10c). In conclusion, we suggest that these volcanic rocks and gabbroic cumulates have the same source – depleted mantle modified by subducted oceanic sediments.

6.2. *Geochronological framework of magmatic rocks in eastern Myanmar and adjacent areas*

Previous studies have reported Late Permian-Early Triassic and Late Triassic igneous rocks in eastern Myanmar (Cong et al., 2021; Gardiner et al., 2016). However, our new geochronological data suggest that there are three stages of magmatism in eastern Myanmar, including Early Carboniferous (Stage I), Late Permian-Early Triassic (Stage II), and Late Triassic (Stage III). To better understand the significance of the magmatism in eastern Myanmar, we compared magmatic ages with those in the adjacent areas, including the SW Yunnan (southwest China), Qiangtang terrane (west China/Central Tibet), Thailand/Laos/Cambodia, and Malaysia/Singapore (Fig. 13).

In the northern extension of the Sukhothai arc in the SW Yunnan, continental arc-related magmatism started at ~ 260 Ma and transitioned into collisional-related magmatism during the Late Triassic (Fig. 13; Cong et al., 2020; Deng et al., 2018; Wang et al., 2018). Although detrital zircon ages indicated that a Late Devonian arc-related magmatism in the SW Yunnan area (Nie et al., 2016), the magmatic rocks have not been found yet. The 315–280 Ma back-arc magmatism is reported in the SW Yunnan (Hennig et al., 2009; Jian et al., 2009; Li et al., 2012; Zhai et al., 2019) and could be connected to the ultramafic–mafic rocks in the Luang Prabang-Nan-Sa Kaeo areas (Hara et al., 2020; Ueno and Hisada, 2001; Wang et al., 2020b).

In the Qiangtang terrane, the Late Devonian-Early Carboniferous igneous rocks were proposed to form in an intra-oceanic arc or continental-arc setting (Dan et al., 2019; Jiang et al., 2015; Liu et al., 2018; Wang et al., 2017). A magmatic lull is observed during the Carboniferous, which is similar to those in the SW Yunnan (Fig. 13). The magmatism during the Early Permian to Triassic was suggested to be related to continued subduction of Paleo-Tethys and subsequent continental collision (Liu et al., 2018; Wang et al., 2017; Zhai et al., 2018).

In Malaysia/Singapore, continental arc-related magmatism, known as Eastern Granite Province, is located east of the Bentong-Raub suture zone and ranges in age from 300 Ma to 250 Ma. Collisional-related magmatism, namely Main Range Granite Province, is located at the west of the suture zone and ranges in age from 230 Ma to 200 Ma (Fig. 13; Wai-Pan Ng et al., 2015a, b; Oliver et al., 2014). The Kyaing Tong granite in eastern Myanmar and some granite plutons in western

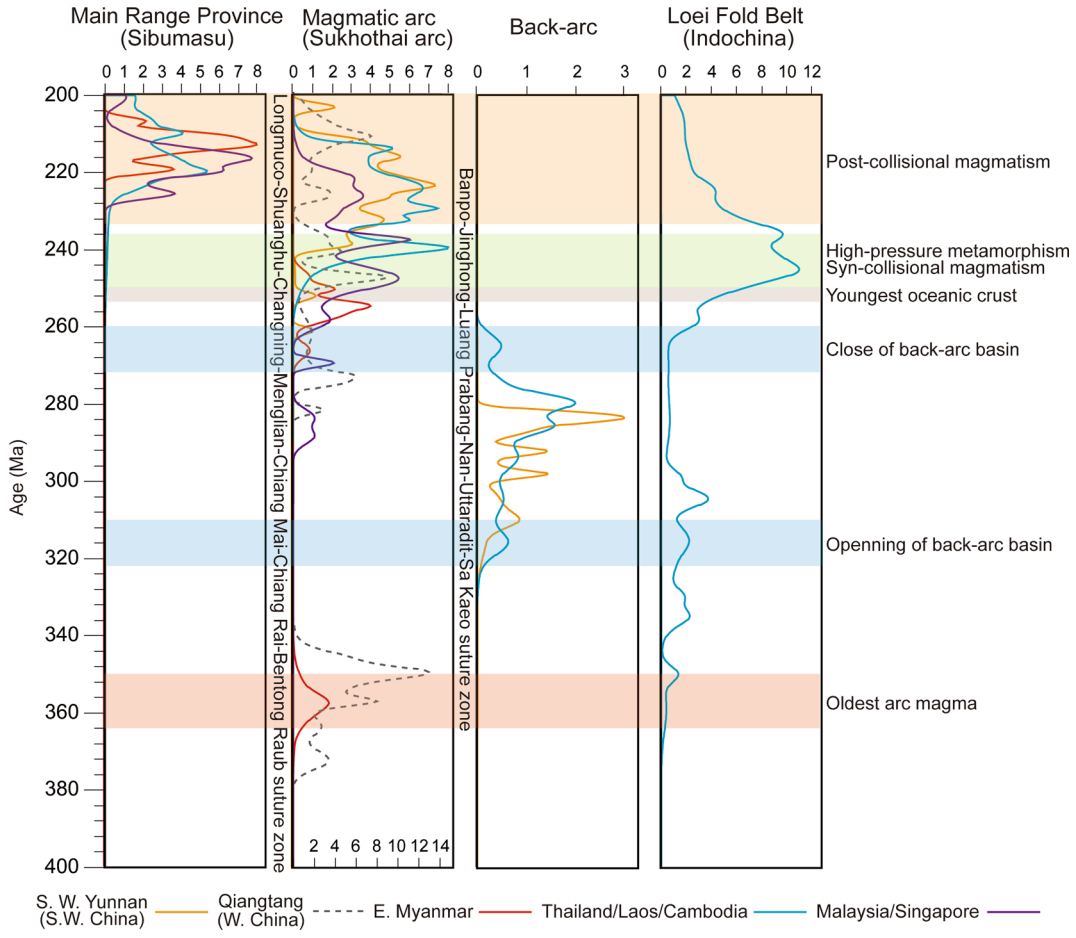

Fig. 13. Probability density plots of the crystallization ages of magmatic rocks from different regions along the Eastern Paleo-Tethys belt. Detailed data sources are listed in Supplementary Table S1.

Thailand also belonging to the Main Range Granite Province were formed during 230–200 Ma (Gardiner et al., 2016; Wang et al., 2016b).

In western Thailand of the Sukhothai terrane, magmatism mainly occurred during 240–210 Ma (Khin Zaw et al., 2014; Wang et al., 2016b, 2018; Khin Zaw and Meffre, 2007; Khositanont and Khin Zaw, 2012), which is a shorter duration than the magmatism in the Qiangtang terrane, SW Yunnan, and in Malaysia/Singapore. Their formation time is slightly later than those in eastern Myanmar (266–246 Ma). In combination with our data, the magmatic rocks in the Sukhothai terrane were mainly formed during the Late Permian to Late Triassic and a magmatic lull during the Carboniferous to Late Permian (Fig. 13). However, detrital zircon ages from the Sukhothai terrane documented magmatic events during the Late Carboniferous to Triassic (Hara et al., 2017).

In Thailand/Laos/Cambodia of the Indochina Block, previous studies recognized a back-arc basin with basaltic rocks and ophiolites formed at 320–260 Ma (Fig. 13; Hara et al., 2020; Metcalfe, 2013; Qian et al., 2016; Y. Wang et al., 2020b), which connects to the SW Yunnan area. It is noteworthy that the 450–400 Ma, 350–300 Ma and 260–240 Ma magmatic rocks located to the east of this back-arc basin is distributed in the Loei Fold Belt of the Indochina Block (Fig. 13; Kamvong et al., 2014; Khin Zaw et al., 2014; Qian et al., 2015; Salam et al., 2014). The Late Ordovician to Early Devonian magmatism in the Loei Fold Belt was thought to be related to the subduction of the Proto-Tethys (Shi et al., 2021). The Carboniferous and Late Permian to Middle Triassic igneous rocks were proposed to form in a continental arc-related setting (Fig. 13; Kamvong et al., 2014; Qian et al., 2015, 2016; Salam et al., 2014; Shi et al., 2021), which are comparable to the magmatic rocks in the Sukhothai arc.

As summarized above, eastern Myanmar has a similar magmatic history to the areas adjacent to the Longmuco-Shuanghu-Changning-Menglian-Chiang Mai-Chiang Rai-Bentong Raub suture zone (Fig. 13). Stage I magmatism in eastern Myanmar is coeval to the arc magmatism in the Qiangtang terrane and is slightly earlier than continental arc magmatism in the western Indochina Block. Stage II and III magmatism in eastern Myanmar is within the range of continental arc and collisional-related magmatism, respectively, in the Qiangtang terrane, and the SW Yunnan, Thailand/Laos/Cambodia and Malaysia/Singapore. It should be noted that there are three branches of the Paleo-Tethys Ocean, including the northern branch (A'nyemaqen-Mianlue suture), central branch (Jinshajiang-Ailaoshan-Song Ma suture), and southern branch (Longmuco-Shuanghu-Changning-Menglian-Chiang Mai-Chiang Rai-Bentong-Raub suture) (Metcalfe, 2021; Wu et al., 2020b). The southern branch sutures are generally accepted to represent the main ocean basin (Gardiner et al., 2016; Metcalfe, 2013, 2021; Wang et al., 2018; Wu et al., 2020b; Zhai et al., 2016). As discussed above, the magmatic histories along the southern branch sutures are similar (Fig. 13). Combined with evidence from paleogeographic and paleomagnetic studies (Ma et al., 2019; Metcalfe, 2021; Wang et al., 2018; Yan et al., 2019; Zhao et al., 2020), we suggest that the geodynamic evolution of the eastern Paleo-Tethys should be considered as a single continuous continental arc system along the ~ 4000 km long belt since the Early Carboniferous.

6.3. Implications for the evolution of the eastern Paleo-Tethys

6.3.1. Early Carboniferous to Middle Permian

The tectonic evolution of the eastern Paleo-Tethys has been extensively debated. The geological and paleomagnetic evidence support that the eastern Paleo-Tethys Ocean have been opened since the Middle Devonian in southeast Asia or even earlier (Cambrian) in the Qiangtang terrane (Feng et al., 2005; Ma et al., 2019; Metcalfe, 2013; Metcalfe et al., 2017; Ueno et al., 2010; Zhai et al., 2016). However, the time of initiation of oceanic subduction has not been well constrained.

The whole-rock geochemical characteristics of ~ 360 Ma mafic rocks show arc-related features with depletion in Nb-Ta and high Th/Yb (>0.8) and low $(Nb/La)_N$ (<0.5) ratios. These geochemical features are distinct from the back-arc basin basalt, which has a low Th/Yb (<0.3) ratio and a high $(Nb/La)_N$ (>0.6) ratio (Pearce et al., 2005), indicating that they are not produced in a back-arc region. Slab break-off or slab tearing during the oceanic subduction will induce upwelling of the deep asthenosphere and produce alkaline magma with OIB features (Ji et al., 2016; Rosenbaum et al., 2018), which is also different with our samples. However, their similar trace-element patterns and REE patterns (Fig. 9a and b) to those Silurian ophiolites from the Changning-Menglian suture zone (Wang et al., 2013) and some of Carboniferous ophiolites in the Longmuco-Shuanghu suture zone (Zhai et al., 2013), suggest that they could be ophiolites of the Paleo-Tethys Oceanic crust. In addition, their outcrop location is near the border between the Sukhothai arc and the southern extension of the Changning-Menglian suture zone. However, compared to the Silurian ophiolites, our samples show more enriched Rb and Th contents, and they are distinct in the Th/Yb vs. Nb/Yb diagram (Fig. 12a). Our samples also show similarities to those Carboniferous and Permian SSZ-type (supra-subduction zone) ophiolites in the Th/Yb vs. Nb/Yb diagram (Fig. 12a). The enrichment of Th is best explained by subduction-related processes (Pearce, 2008). According to Grimes et al. (2015), zircon geochemistry could help discriminate SSZ-type ophiolites and volcanic arc-type ophiolites. Our samples are all plotted into the arc-related setting (Fig. 12e and f); therefore, they are not SSZ-type ophiolites. In any case, our samples indicate that the subduction of the Paleo-Tethys had occurred. On the basis of the captured zircons from the coeval trondhjemitic dikes, we prefer a continental arc setting. Therefore, we suggest that the subduction of the eastern Paleo-Tethys began by ~ 360 Ma in eastern Myanmar along a continental margin (Fig. 14a and d).

According to studies in the Qiangtang terrane, researchers have proposed that the subduction of eastern Paleo-Tethys lasted from the Late Devonian to the Triassic (Dan et al., 2019; Liu et al., 2018; Wang et al., 2017; Zhai et al., 2016, 2018). Data from the SW Yunnan and Southeast Asia indicates that subduction of the Paleo-Tethys began at least since ~ 300 Ma (Deng et al., 2018; Gardiner et al., 2016; Metcalfe, 2013; Wang et al., 2018). Detrital zircon ages in SW Yunnan documented arc-related magmatism during the Late Devonian (Nie et al., 2016). Combining the above evidence with our new findings, we propose that subduction of the eastern Paleo-Tethys would have started along the Longmuco-Shuanghu-Changning-Menglian-Chiang Mai-Chiang Rai-Bentong Raub sutures since Early Carboniferous (Fig. 14a and d). We consider that extensive arc-related magmatic rocks formed during the Early Carboniferous to Early Carboniferous extending ~ 4000 km belt.

In the Loei Fold Belt, there is also magmatic rocks formed during the Carboniferous, showing arc-related geochemical characteristics (Kamvong et al., 2014; Qian et al., 2015, 2016; Shi et al., 2021). During this period, the back-arc basin between the Sukhothai arc and Indochina Block had not opened (Metcalfe, 2021; Qian et al., 2015, 2016; Shi et al., 2021). Moreover, there is a "magmatic lull" in the Sukhothai arc during the Late Carboniferous (Fig. 13). According to the above observations, we suggest that the eastwardly migrating magmatism from the Sukhothai arc to the Loei Fold Belt may be related to a low-angle to flat subduction of the Paleo-Tethys during 360–320 Ma. Numerical studies revealed that a young and thin oceanic slab will lead to steep subduction (Hu and Gurnis, 2020; Huangfu et al., 2016). Flat subduction could be achieved by increasing slab thickness and slab age, although many other factors may also influence the slab dip (Hu and Gurnis, 2020; Huangfu et al., 2016; Lallemand et al., 2005). During 320–280 Ma, magmatism migrated westward, and the back-arc basin began to open during this stage (Fig. 13), which reflects a slab roll-back process. The timespan of magmatism in the back-arc basin is also coeval to the magmatic gap in the Indochina block (Fig. 12). This could be explained by high angle subduction (Fig. 14b and e).

6.3.2. Late Permian to Late Triassic

The Late Permian volcanic rocks in this study with depleted isotopic

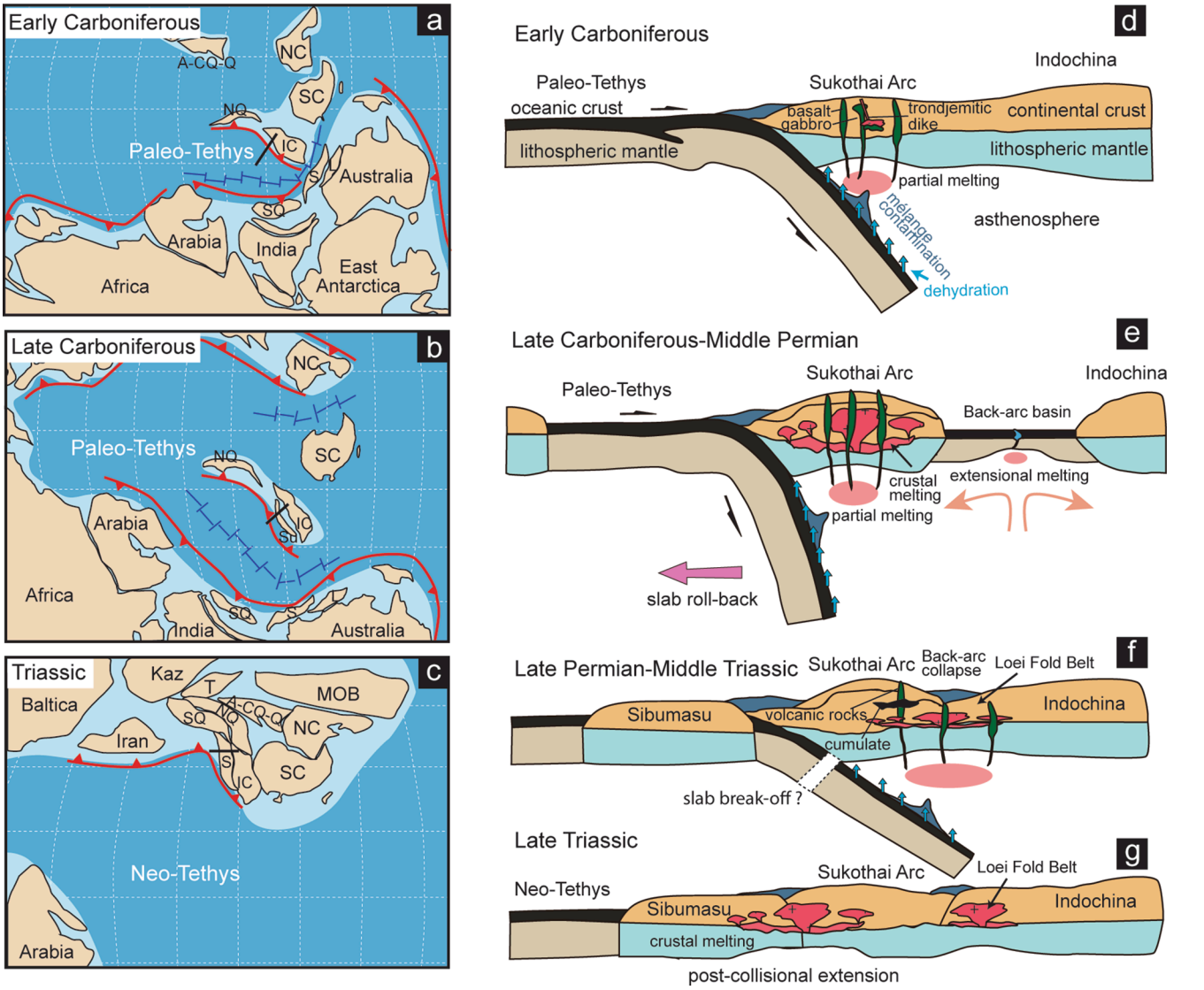

Fig. 14. Schematic diagram of the tectonic evolution model from Early Carboniferous to Late Triassic in eastern Myanmar and adjacent area (not to scale). (a-c) The paleogeographic map of the blocks related to the Eastern Paleo-Tethys during the Early Carboniferous, the Late Carboniferous, and the Late Triassic. The paleogeographic map is modified from Huang et al. (2018) and Zhao et al. (2018, 2020). Abbreviations: T, Tarim Craton; A-CQ-Q, Alax-Central Qilian-Qaidam terrane; NC, North China Craton; SC, South China Craton; NQ, North Qiangtang terrane; IC, Indochina terrane; S, Sibumasu terrane; L, Lhasa terrane; SQ, South Qiangtang terrane; Su, Sukhothai arc terrane; Kaz, Kazhakstan. (d) The subduction of the Paleo-Tethys has started during the Early Carboniferous. (e) The continued subduction during the Late Carboniferous to Middle Permian and related back-arc extension. (f) Tectonic transition from subduction to collision during the Late Permian to Middle Triassic. (g) The post-collisional extension during the Late Triassic.

composition showed similar geochemical features to the widespread Late Permian volcanic rocks from the Qiangtang terrane to Malaysia/Singapore (Wang et al., 2017, 2018), indicating that subduction continued during the Late Permian (Fig. 13). Previous studies mainly accepted that the collision between the Indochina and Sibumasu Blocks occurred during the Middle Triassic (e.g., Sone and Metcalfe, 2008; Wang et al., 2018). This is mainly evidenced by the deep-water sedimentation, oceanic/pelagic sedimentary records up till the Ladinian, and the earliest igneous rock (~237 Ma) in the Main Range Granite Province (e.g., Sone and Metcalfe, 2008; Wang et al., 2018). In addition, the Early-Middle Triassic volcanic rocks of the Sukhothai arc in Thailand showed subduction-related geochemical features and were believed to have generated during the subduction-collision transition (Wang et al., 2018). However, deep-water sedimentation could exist after the initial collision, as suggested by Hu et al. (2016). The magmatism in the Main Range Granite Province on the passive margin indicated that the collision should have occurred before the ~ 237 Ma. The Lancang Group, which is composed of fore-arc sediments, and continental rocks underwent 238–234 Ma high-pressure metamorphism, indicating that the initial collision have started before ~ 238–234 Ma (Wang et al., 2020a, 2021). According to the study by Metcalfe et al. (2017) on the Inthanon Zone, the initial collision may have happened during the Late Permian. The missing of uppermost Permian strata along the Changning-Menglian zone (Nakazawa et al., 2009; Wang et al., 2018) indicates that the initial tectonic uplift during the Late Permian. A recent paleomagnetic study further showed that the collision between the Indochina and Sibumasu Blocks occurred during the Late Permian to Early Triassic (Zhao et al., 2020). In addition, a recent study on isotope and trace elements of detrital zircons suggested that the collision between the Indochina and Sibumasu Blocks was at ~ 255 Ma in Thailand, ~20 Myr earlier than in Malaysia (Liu et al., 2022). Therefore, we suggest that the initial collision could have happened during the Early Triassic. The Early-Middle Triassic volcanic rocks in Thailand with subduction-related geochemical features reflect the oceanic slab may be not fully detached before the

Middle Triassic.

The close spatial relationship and simultaneous magmatism in the Sukhothai terrane and Loei Fold Belt (Cong et al., 2021; Khin Zaw et al., 2014) indicate that they were most likely to have formed in the same subduction-related setting. Although recent studies proposed an eastward subduction of the Nan back-arc oceanic slab (Jiang et al., 2021; Shi et al., 2021), the lack of oceanic eclogite questioned the existence of this subduction zone. The collapse of the back-arc basin and possible arc-continent collision during the Late Permian-Early Triassic could have been caused by the eastward advancing subduction of the Paleo-Tethys. Therefore, we suggested that the Late Permian to Middle Triassic magmatism along the entire belt were formed in a tectonic transition of the Paleo-Tethys from subduction to continental collision (Fig. 14c and g). This scheme is similar to the proposed closure process of the Paleo-Tethys based on the Jinshajiang segment (Zi et al., 2013). The Late Triassic granites in the Main Range Granite Province is a typical product of post-collisional magmatism (Oliver et al., 2014; Wai-Pan Ng et al., 2015b), which is distributed in the passive margin (Fig. 14c and g). Therefore, the continental collision between the Indochina and Sibumasu may have occurred during 250–240 Ma.

7. Conclusions

(1) Integrating our new data with previous studies, magmatic activity in eastern Myanmar could be divided into three stages, that is Early Carboniferous (360–355 Ma), Late Permian to Early Triassic (266–247 Ma), and Late Triassic (220–210 Ma).

(2) The 360–357 Ma basaltic rocks were derived from partial melting of mélange diapir mixed with peridotite and experienced assimilation and fractional crystallization during magma ascent. The 357–355 Ma trondhjemitic dikes were derived from partial melting of the basaltic rocks and experienced fractional crystallization at low-pressure conditions. The 257–255 Ma volcanic rocks underwent magma assimilation and fractional crystallization and were formed by partial melting of the depleted mantle wedge, which was modified by oceanic sediments. The gabbroic cumulates are products of late-phase fractional crystallization during magma ascent.

(3) The three stages of magmatism described for eastern Myanmar could correspond to magmatism in the Central Tibet, SW Yunnan, and Southeast Asia. Together, these magmatic records suggest that the entire ~ 4000 km long eastern Paleo-Tethys belt shares a common evolutionary history.

(4) Early Carboniferous magmatism in eastern Myanmar is related to the subduction of the Paleo-Tethys along the western continental margin of the Indochina Block. The continued subduction may have caused the back-arc opening during the Late Carboniferous and subsequently resulted in extensive magmatism along the entire eastern Paleo-Tethys belt since the Permian. Subduction continued during the Late Permian and the final amalgamation between the Sibumasu and Indochina occurred during the Early Triassic.

CRediT authorship contribution statement

Fangyang Hu: Writing – original draft, Visualization, Methodology, Conceptualization, Funding acquisition. **Fu-Yuan Wu:** Supervision, Investigation, Conceptualization, Funding acquisition. **Jian-Gang Wang:** Investigation. **Mihai N. Ducea:** Writing – review & editing, Funding acquisition. **James B. Chapman:** Writing – review & editing. **Khin Zaw:** Writing – review & editing. **Wei Lin:** Investigation. **Kyaing Sein:** Investigation. **Sebastien Meffre:** Writing – review & editing.

Declaration of Competing Interest

The authors declare that they have no known competing financial interests or personal relationships that could have appeared to influence the work reported in this paper.

Acknowledgments

We are highly indebted to journal reviewers (Jian-Wei Zi and an anonymous reviewer) and editors for their insightful comments and suggestions to improve the manuscript. We also want to thank Lihui Jia for assistance during mineral electron microprobe analyses, Shitou Wu for LA-ICP-MS zircon U-Th-Pb isotopic analyses, Chao Huang for MC-LA-ICP-MS zircon Hf isotopic analyses, Xiaoxiao Ling and Guoqiang Tang for assistance with SIMS zircon U–Pb–O isotopic analyses at the Institute of Geology and Geophysics, Chinese Academy of Science in Beijing. F.Y. H. and F.Y.W. acknowledges support from the National Natural Science Foundation of China [91755000, 41888101, 41902055], and China Postdoctoral Science Foundation [2018M640177]. M.N.D. acknowledges support from US National Science Foundation [EAR 1725002] and the Romanian Executive Agency for Higher Education, Research, Development and Innovation Funding (UEFISCDI) project [PN-III-P4-ID-PCCF-2016-0014].

Appendix A. Supplementary material

Supplementary data to this article can be found online at https://doi.org/10.1016/j.jseaes.2022.105093.

References

Amelin, Y., Lee, D.-C., Halliday, A.N., 2000. Early-middle archaean crustal evolution deduced from Lu-Hf and U-Pb isotopic studies of single zircon grains. Geochim. Cosmochim. Acta 64 (24), 4205–4225. https://doi.org/10.1016/S0016-7037(00)00493-2.

Arboit, F., Collins, A.S., Morley, C.K., King, R., Amrouch, K., 2016. Detrital zircon analysis of the southwest Indochina terrane, central Thailand: Unravelling the Indosinian orogeny. GSA Bulletin 128 (5-6), 1024–1043. https://doi.org/10.1130/B31411.110.1130/2016044.

Barker, F., 1979. Chapter 1 - Trondhjemite: Definition, Environment and Hypotheses of Origin. In: Barker, F. (Ed.), Developments in Petrology, Trondhjemites, Dacites, and Related Rocks. Elsevier, pp. 1–12. https://doi.org/10.1016/B978-0-444-41765-7.50006-X.

Bas, M.J.L., Maitre, R.W.L., Streckeisen, A., Zanettin, B., IUGS Subcommission on the Systematics of Igneous Rocks, 1986. A Chemical Classification of Volcanic Rocks Based on the Total Alkali-Silica Diagram. Journal of Petrology 27, 745–750. https://doi.org/10.1093/petrology/27.3.745.

Blichert-Toft, J., Albarède, F., 1997. The Lu-Hf isotope geochemistry of chondrites and the evolution of the mantle-crust system. Earth Planet. Sci. Lett. 148 (1-2), 243–258. https://doi.org/10.1016/S0012-821X(97)00040-X.

Chauvel, C., Garçon, M., Bureau, S., Besnault, A., Jahn, B., Ding, Z., 2014. Constraints from loess on the Hf–Nd isotopic composition of the upper continental crust. Earth Planet. Sci. Lett. 388, 48–58. https://doi.org/10.1016/j.epsl.2013.11.045.

Chauvel, C., Lewin, E., Carpentier, M., Arndt, N.T., Marini, J.-C., 2008. Role of recycled oceanic basalt and sediment in generating the Hf–Nd mantle array. Nat. Geosci. 1, 64–67. https://doi.org/10.1038/ngeo.2007.51.

Chauvel, C., Marini, J.-C., Plank, T., Ludden, J.N., 2009. Hf-Nd input flux in the Izu-Mariana subduction zone and recycling of subducted material in the mantle. Geochem. Geophys. Geosyst. 10 (1), n/a–n/a. https://doi.org/10.1029/2008GC002101.

Cong, F., Wu, F.-Y., Li, W.-C., Mou, C.-L., Huang, X.-M., Wang, B.-D., Hu, F.-Y., Peng, Z.-M., 2020. Origin of the Triassic Lincang granites in the southeastern Tibetan Plateau: Crystallization from crystal mush. Lithos 360-361, 105452. https://doi.org/10.1016/j.lithos.2020.105452.

Cong, F., Wu, F.-Y., Li, W.-C., Wang, J.-G., Hu, F.-Y., He, D.-F., Ji, W.-Q., Lin, W., Sein, K., 2021. Petrogenesis of the Main Range and Eastern Province granites in eastern Myanmar: New insights from zircon U-Pb ages and Sr–Nd isotopes. Lithos 382-383, 105895. https://doi.org/10.1016/j.lithos.2020.105895.

Cooper, G.F., Blundy, J.D., Macpherson, C.G., Humphreys, M.C.S., Davidson, J.P., 2019. Evidence from plutonic xenoliths for magma differentiation, mixing and storage in a volatile-rich crystal mush beneath St. Eustatius, Lesser Antilles. Contrib Mineral Petrol 174, 39. https://doi.org/10.1007/s00410-019-1576-4.

Cooper, G.F., Davidson, J.P., Blundy, J.D., 2016. Plutonic xenoliths from Martinique, Lesser Antilles: evidence for open system processes and reactive melt flow in island arc crust. Contrib Mineral Petrol 171, 87. https://doi.org/10.1007/s00410-016-1299-8.

Corfu, F., Hanchar, J.M., Hoskin, P.W.O., Kinny, P., 2003. Atlas of zircon textures. Rev. Mineral. Geochem. 53, 469–500.

Dan, W., Wang, Q., Li, X.-H., Tang, G.-J., Zhang, C., Zhang, X.-Z., Wang, J., 2019. Low δ18O magmas in the carboniferous intra-oceanic arc, central Tibet: Implications for felsic magma generation and oceanic arc accretion. Lithos 326–327, 28–38. https://doi.org/10.1016/j.lithos.2018.12.011.

Dan, W., Wang, Q., Zhang, X.-Z., Zhang, C., Tang, G.-J., Wang, J., Ou, Q., Hao, L.-L., Qi, Y., 2018. Magmatic record of Late Devonian arc-continent collision in the

northern Qiangtang, Tibet: Implications for the early evolution of East Paleo-Tethys Ocean. Lithos 308–309, 104–117. https://doi.org/10.1016/j.lithos.2018.03.002.
Deng, J., Wang, C., Zi, J.-W., Xia, R., Li, Q., 2018. Constraining subduction-collision processes of the Paleo-Tethys along the Changning-Menglian Suture: New zircon U-Pb ages and Sr–Nd–Pb–Hf–O isotopes of the Lincang Batholith. Gondwana Research, Tectono-Magmatic Evolution and Metallogenesis in the eastern Tethyan orogens 62, 75–92. https://doi.org/10.1016/j.gr.2017.10.008.
Dew, R.E.C., Collins, A.S., Glorie, S., Morley, C.K., Blades, M.L., Nachtergaele, S., King, R., Foden, J., De Grave, J., Kanjanapayont, P., Evans, N.J., Alessio, B.L., Charusiri, P., 2018. Probing into Thailand's basement: New insights from U-Pb geochronology, Sr, Sm–Nd, Pb and Lu–Hf isotopic systems from granitoids. Lithos 320–321, 332–354. https://doi.org/10.1016/j.lithos.2018.09.019.
Duan, X.D., Li, J., Zeng, W.T., Feng, W.J., 2006. The discovery of Ganlongtang tectonic melange in the middle section of Changning-Menglian zone. Yunnan Geology 25, 53–62 in Chinese with English abstract.
Feng, Q.-L., 2002. Stratigraphy of volcanic rocks in the Changning-Menglian Belt in southwestern Yunnan, China. Journal of Asian Earth Sciences, Permian of Southeast Asia 20 (6), 657–664. https://doi.org/10.1016/S1367-9120(02)00006-8.
Feng, Q., Malila, K., Wonganan, N., Chonglakmani, C., Helmcke, D., Ingavat-Helmcke, R., Caridroit, M., 2005. Permian and Triassic Radiolaria from Northwest Thailand: paleogeographical implications. Rev. Micropaléontol. 48 (4), 237–255. https://doi.org/10.1016/j.revmic.2005.09.004.
Fiannacca, P., Basei, M.A.S., Cirrincione, R., Pezzino, A., Russo, D., 2020. Water-assisted production of late-orogenic trondhjemites at magmatic and subsolidus conditions. Geological Society, London, Special Publications 491 (1), 147–178. https://doi.org/10.1144/SP491-2018-113.
Freund, S., Haase, K.M., Keith, M., Beier, C., Garbe-Schönberg, D., 2014. Constraints on the formation of geochemically variable plagiogranite intrusions in the Troodos Ophiolite. Cyprus. Contrib Mineral Petrol 167, 978. https://doi.org/10.1007/s00410-014-0978-6.
Gardiner, N.J., Searle, M.P., Morley, C.K., Whitehouse, M.P., Spencer, C.J., Robb, L.J., 2016. The closure of Palaeo-Tethys in Eastern Myanmar and Northern Thailand: New insights from zircon U-Pb and Hf isotope data. Gondwana Res. 39, 401–422. https://doi.org/10.1016/j.gr.2015.03.001.
Geisler, T., Schaltegger, U., Tomaschek, F., 2007. Re-equilibration of Zircon in Aqueous Fluids and Melts. Elements 3 (1), 43–50. https://doi.org/10.2113/gselements.3.1.43.
Griffin, W.L., Pearson, N.J., Belousova, E., Jackson, S.E., van Achterbergh, E., O'Reilly, S. Y., Shee, S.R., 2000. The Hf isotope composition of cratonic mantle: LAM-MC-ICPMS analysis of zircon megacrysts in kimberlites. Geochim. Cosmochim. Acta 64 (1), 133–147. https://doi.org/10.1016/S0016-7037(99)00343-9.
Grimes, C.B., Wooden, J.L., Cheadle, M.J., John, B.E., 2015. "Fingerprinting" tectono-magmatic provenance using trace elements in igneous zircon. Contrib Mineral Petrol 170, 46. https://doi.org/10.1007/s00410-015-1199-3.
Haase, K.M., Freund, S., Beier, C., Koepke, J., Erdmann, M., Hauff, F., 2016. Constraints on the magmatic evolution of the oceanic crust from plagiogranite intrusions in the Oman ophiolite. Contrib Mineral Petrol 171, 46. https://doi.org/10.1007/s00410-016-1261-9.
Halpin, J.A., Daczko, N.R., Milan, L.A., Clarke, G.L., 2012. Decoding near-concordant U-Pb zircon ages spanning several hundred million years: recrystallisation, metamictisation or diffusion? Contrib Mineral Petrol 163 (1), 67–85. https://doi.org/10.1007/s00410-011-0659-7.
Hara, H., Ito, T., Tokiwa, T., Kong, S., Lim, P., 2020. The origin of the Pailin Crystalline Complex in western Cambodia, and back-arc basin development in the Paleo-Tethys Ocean. Gondwana Res. 82, 299–316. https://doi.org/10.1016/j.gr.2020.01.007.
Hara, H., Kunii, M., Miyake, Y., Hisada, K., Kamata, Y., Ueno, K., Kon, Y., Kurihara, T., Ueda, H., Assavapatchara, S., Treerotchananon, A., Charoentitirat, T., Charusiri, P., 2017. Sandstone provenance and U-Pb ages of detrital zircons from Permian-Triassic forearc sediments within the Sukhothai Arc, northern Thailand: Record of volcanic-arc evolution in response to Paleo-Tethys subduction. J. Asian Earth Sci. 146, 30–55. https://doi.org/10.1016/j.jseaes.2017.04.021.
Hastie, A.R., Kerr, A.C., Pearce, J.A., Mitchell, S.F., 2007. Classification of Altered Volcanic Island Arc Rocks using Immobile Trace Elements: Development of the Th–Co Discrimination Diagram. J Petrology 48, 2341–2357. https://doi.org/10.1093/petrology/egm062.
Hawthorne, F.C., Oberti, R., Harlow, G.E., Maresch, W.V., Martin, R.F., Schumacher, J. C., Welch, M.D., 2012. Nomenclature of the amphibole supergroup. Am. Mineral. 97 (11-12), 2031–2048. https://doi.org/10.2138/am.2012.4276.
Hennig, D., Lehmann, B., Frei, D., Belyatsky, B., Zhao, X.F., Cabral, A.R., Zeng, P.S., Zhou, M.F., Schmidt, K., 2009. Early Permian seafloor to continental arc magmatism in the eastern Paleo-Tethys: U-Pb age and Nd–Sr isotope data from the southern Lancangjiang zone, Yunnan, China. Lithos 113 (3-4), 408–422. https://doi.org/10.1016/j.lithos.2009.04.031.
Holland, T., Blundy, J., 1994. Non-ideal interactions in calcic amphiboles and their bearing on amphibole-plagioclase thermometry. Contr. Mineral. and Petrol. 116 (4), 433–447. https://doi.org/10.1007/BF00310910.
Hoskin, P. w. o., Black, L. p., 2000. Metamorphic zircon formation by solid-state recrystallization of protolith igneous zircon. Journal of Metamorphic Geology 18, 423–439. https://doi.org/10.1046/j.1525-1314.2000.00266.x.
Hu, F., Liu, S., Ducea, M.N., Chapman, J.B., Wu, F., Kusky, T., 2020. Early Mesozoic magmatism and tectonic evolution of the Qinling Orogen: Implications for oblique continental collision. Gondwana Res. 88, 296–332. https://doi.org/10.1016/j.gr.2020.07.006.
Hu, J., Gurnis, M., 2020. Subduction Duration and Slab Dip. Geochemistry, Geophysics, Geosystems 21, e2019GC008862. https://doi.org/10.1029/2019GC008862.
Hu, X., Garzanti, E., Wang, J., Huang, W., An, W., Webb, A., 2016. The timing of India-Asia collision onset – Facts, theories, controversies. Earth Sci. Rev. 160, 264–299. https://doi.org/10.1016/j.earscirev.2016.07.014.
Huang, B., Yan, Y., Piper, J.D.A., Zhang, D., Yi, Z., Yu, S., Zhou, T., 2018. Paleomagnetic constraints on the paleogeography of the East Asian blocks during Late Paleozoic and Early Mesozoic times. Earth-Science Reviews, Reconstruction of East Asian Continental Blocks in Pangea 186, 8–36. https://doi.org/10.1016/j.earscirev.2018.02.004.
Huangfu, P., Wang, Y., Cawood, P.A., Li, Z.-H., Fan, W., Gerya, T.V., 2016. Thermo-mechanical controls of flat subduction: Insights from numerical modeling. Gondwana Res. 40, 170–183. https://doi.org/10.1016/j.gr.2016.08.012.
Ji, W.-Q., Wu, F.-Y., Chung, S.-L., Wang, X.-C., Liu, C.-Z., Li, Q.-L., Liu, Z.-C., Liu, X.-C., Wang, J.-G., 2016. Eocene Neo-Tethyan slab breakoff constrained by 45 Ma oceanic island basalt–type magmatism in southern Tibet. Geology 44 (4), 283–286. https://doi.org/10.1130/G37612.110.1130/2016087.
Jian, P., Liu, D., Kröner, A., Zhang, Q.i., Wang, Y., Sun, X., Zhang, W., 2009. Devonian to Permian plate tectonic cycle of the Paleo-Tethys Orogen in southwest China (II): Insights from zircon ages of ophiolites, arc/back-arc assemblages and within-plate igneous rocks and generation of the Emeishan CFB province. Lithos 113 (3-4), 767–784. https://doi.org/10.1016/j.lithos.2009.04.006.
Jiang, H., Li, W.-Q., Zhao, K.-D., Zhang, D.i., Jiang, S.-Y., 2021. Middle Triassic diorites from the Loei Fold Belt, NE Thailand: Petrogenesis and tectonic implications in the context of Paleotethyan subduction. Lithos 382-383, 105955. https://doi.org/10.1016/j.lithos.2020.105955.
Jiang, Q., Li, C., Su, L., Hu, P., Xie, C., Wu, H., 2015. Carboniferous arc magmatism in the Qiangtang area, northern Tibet: Zircon U-Pb ages, geochemical and Lu–Hf isotopic characteristics, and tectonic implications. J. Asian Earth Sci. 100, 132–144. https://doi.org/10.1016/j.jseaes.2015.01.012.
Kamvong, T., Khin Zaw, Meffre, S., Maas, R., Stein, H., Lai, C.-K., 2014. Adakites in the Truong Son and Loei fold belts, Thailand and Laos: Genesis and implications for geodynamics and metallogeny. Gondwana Res. 26, 165–184. https://doi.org/10.1016/j.gr.2013.06.011.
Kawamoto, T., 1996. Experimental constraints on differentiation and H2O abundance of calc-alkaline magmas. Earth Planet. Sci. Lett. 144 (3-4), 577–589. https://doi.org/10.1016/S0012-821X(96)00182-3.
Kelemen, P.B., Hanghøj, K., Greene, A.R., 2003. One View of the Geochemistry of Subduction-related Magmatic Arcs, with an Emphasis on Primitive Andesite and Lower Crust. Treatise on Geochemistry. Elsevier 593–659.
Khin Zaw, 1990. Geological, petrological and geochemical characteristics of granitoid rocks in Burma: With special reference to the associated W-Sn mineralization and their tectonic setting. J. SE Asian Earth Sci. 4, 293–335. https://doi.org/10.1016/0743-9547(90)90004-W.
Khin Zaw, Meffre, S., 2007. Higher degree students, Metallogenic Relations and Deposit-scale Studies, Final Report. Geochronology, Metallogenesis and Deposit Styles of Loei Fold Belt in Thailand and Laos PDR. ARC Linkage Project, Final Report. CODES with Industry Partners University of Tasmania, Hobart.
Khin Zaw, Meffre, S., Lai, C.-K., Burrett, C., Santosh, M., Graham, I., Manaka, T., Salam, A., Kamvong, T., Cromie, P., 2014. Tectonics and metallogeny of mainland Southeast Asia — A review and contribution. Gondwana Res. 26, 5–30. https://doi.org/10.1016/j.gr.2013.10.010.
Khositanont, S., Khin Zaw, 2012. Geochemical characteristics and U-Pb zircon age determination of the Lampang-Phrae volcanic belt: Implication for tectonic evolution of the Shan-Thai Terrane. Abstract Volume, First International Conference on Myanmar Geology, 1-2 March 2012, Sedona Hotel, Yangon, Myanmar.
Lallemand, S., Heuret, A., Boutelier, D., 2005. On the relationships between slab dip, back-arc stress, upper plate absolute motion, and crustal nature in subduction zones. Geochem. Geophys. Geosyst. 6 (9), n/a–n/a. https://doi.org/10.1029/2005GC000917.
Li, G., Li, C., Ripley, E.M., Kamo, S., Su, S., 2012. Geochronology, petrology and geochemistry of the Nanlinshan and Banpo mafic–ultramafic intrusions: implications for subduction initiation in the eastern Paleo-Tethys. Contrib Mineral Petrol 164 (5), 773–788. https://doi.org/10.1007/s00410-012-0770-4.
Liu, G., Sun, Z., Zi, J., Santosh, M., Zhao, T., Feng, Q., Chen, G., Nie, X., Li, J., Zhang, S., 2021. Proto-Tethys ophiolitic mélange in SW Yunnan: Constraints from zircon U-Pb geochronology and geochemistry. Geosci. Front. 12 (5), 101200. https://doi.org/10.1016/j.gsf.2021.101200.
Liu, H., McKenzie, N.R., Colleps, C.L., Chen, W., Ying, Y., Stockli, L., Sardsud, A., Stockli, D.F., 2022. Zircon isotope–trace element compositions track Paleozoic-Mesozoic slab dynamics and terrane accretion in Southeast Asia. Earth Planet. Sci. Lett. 578, 117298. https://doi.org/10.1016/j.epsl.2021.117298.
Liu, J.-H., Xie, C.-M., Li, C., Wang, M., Wu, H., Li, X.-K., Liu, Y.-M., Zhang, T.-Y., 2018. Early Carboniferous adakite-like and I-type granites in central Qiangtang, northern Tibet: Implications for intra-oceanic subduction and back-arc basin formation within the Paleo-Tethys Ocean. Lithos 296–299, 265–280. https://doi.org/10.1016/j.lithos.2017.11.005.
Ma, Y., Wang, Q., Wang, J., Yang, T., Tan, X., Dan, W., Zhang, X., Ma, L., Wang, Z., Hu, W., Zhang, S., Wu, H., Li, H., Cao, L., 2019. Paleomagnetic Constraints on the Origin and Drift History of the North Qiangtang Terrane in the Late Paleozoic. Geophys. Res. Lett. 46 (2), 689–697. https://doi.org/10.1029/2018GL080964.
Marien, C.S., Hoffmann, J.E., Garbe-Schönberg, C.-D., Münker, C., 2019. Petrogenesis of plagiogranites from the Troodos Ophiolite Complex. Cyprus. Contrib Mineral Petrol 174, 35. https://doi.org/10.1007/s00410-019-1569-3.
Marschall, H.R., Schumacher, J.C., 2012. Arc magmas sourced from mélange diapirs in subduction zones. Nat. Geosci. 5 (12), 862–867. https://doi.org/10.1038/ngeo1634.
Martin, H., Smithies, R.H., Rapp, R., Moyen, J.-F., Champion, D., 2005. An overview of adakite, tonalite–trondhjemite–granodiorite (TTG), and sanukitoid: relationships

and some implications for crustal evolution. Lithos 79 (1-2), 1–24. https://doi.org/10.1016/j.lithos.2004.04.048.
Melekhova, E., Blundy, J., Robertson, R., Humphreys, M.C.S., 2015. Experimental Evidence for Polybaric Differentiation of Primitive Arc Basalt beneath St. Vincent. Lesser Antilles. J Petrology 56 (1), 161–192. https://doi.org/10.1093/petrology/egu074.
Metcalfe, I., 2013. Gondwana dispersion and Asian accretion: Tectonic and palaeogeographic evolution of eastern Tethys. J. Asian Earth Sci. 66, 1–33. https://doi.org/10.1016/j.jseaes.2012.12.020.
Metcalfe, I., 2021. Multiple Tethyan ocean basins and orogenic belts in Asia. Gondwana Res. 100, 87–130. https://doi.org/10.1016/j.gr.2021.01.012.
Metcalfe, I., Henderson, C.M., Wakita, K., 2017. Lower Permian conodonts from Palaeo-Tethys Ocean Plate Stratigraphy in the Chiang Mai-Chiang Rai Suture Zone, northern Thailand. Gondwana Res. 44, 54–66. https://doi.org/10.1016/j.gr.2016.12.003.
Miller, C.F., McDowell, S.M., Mapes, R.W., 2003. Hot and cold granites? Implications of zircon saturation temperatures and preservation of inheritance. Geology 31 (6), 529. https://doi.org/10.1130/0091-7613(2003)031<0529:HACGIO>2.0.CO;2.
Minn Chit Thu, 2012. The study of the manganese mineralization at the Ahr-ye village, Tachileik township, Shan State. Yangon University, Yangon, Myanmar. Unpublished MSc thesis.
Mitchell, A., 2018. In: Geological Belts, Plate Boundaries, and Mineral Deposits in Myanmar. Elsevier, pp. 77–96. https://doi.org/10.1016/B978-0-12-803382-1.00003-1.
Morimoto, N., 1988. Nomenclature of PyroxenesDie Nomenklatur von Pyroxenen. Mineral. Petrol. 39 (1), 55–76.
Nakazawa, T., Ueno, K., Wang, X., 2009. Sedimentary facies of Carboniferous-Permian mid-oceanic carbonates in the Changning-Menglian Belt, West Yunnan, Southwest China: Origin and depositional process. Isl. Arc 18, 94–107. https://doi.org/10.1111/j.1440-1738.2008.00650.x.
Nandedkar, R.H., Ulmer, P., Müntener, O., 2014. Fractional crystallization of primitive, hydrous arc magmas: an experimental study at 0.7 GPa. Contrib Mineral Petrol 167, 1–27. https://doi.org/10.1007/s00410-014-1015-5.
Nie, X., Feng, Q., Metcalfe, I., Baxter, A.T., Liu, G., 2016. Discovery of a Late Devonian magmatic arc in the southern Lancangjiang zone, western Yunnan: Geochemical and zircon U-Pb geochronological constraints on the evolution of Tethyan ocean basins in SW China. J. Asian Earth Sci. 118, 32–50. https://doi.org/10.1016/j.jseaes.2015.12.026.
Nielsen, S.G., Marschall, H.R., 2017. Geochemical evidence for mélange melting in global arcs. Sci. Adv. 3, e1602402 https://doi.org/10.1126/sciadv.1602402.
Oliver, G., Khin Zaw, Hotson, M., Meffre, S., Manka, T., 2014. U-Pb zircon geochronology of Early Permian to Late Triassic rocks from Singapore and Johor: A plate tectonic reinterpretation. Gondwana Res. 26 (1), 132–143. https://doi.org/10.1016/j.gr.2013.03.019.
Pearce, J.A., 2008. Geochemical fingerprinting of oceanic basalts with applications to ophiolite classification and the search for Archean oceanic crust. Lithos, Links Between Ophiolites and LIPs in Earth History 100 (1-4), 14–48. https://doi.org/10.1016/j.lithos.2007.06.016.
Pearce, J.A., Norry, M.J., 1979. Petrogenetic implications of Ti, Zr, Y, and Nb variations in volcanic rocks. Contr. Mineral. and Petrol. 69 (1), 33–47. https://doi.org/10.1007/BF00375192.
Pearce, J.A., Stern, R.J., Bloomer, S.H., Fryer, P., 2005. Geochemical mapping of the Mariana arc-basin system: Implications for the nature and distribution of subduction components. Geochem. Geophys. Geosyst. 6 (7), n/a–n/a. https://doi.org/10.1029/2004GC000895.
Peng, Z., Fu, Y., Wang, G., Guan, J., Geng, Q., Hu, J., Liu, Y., Zhang, Z., 2020. The results of geochronological, geochemical and Sr- Nd- Hf isotopic investigations on amphibolites in the Qingping Region, Changning- Menglian Suture Zone. Acta Geol. Sin. 94, 511–526 in Chinese with English abstract.
Pullen, A., Kapp, P., Gehrels, G.E., Vervoort, J.D., Ding, L., 2008. Triassic continental subduction in central Tibet and Mediterranean-style closure of the Paleo-Tethys Ocean. Geology 36 (5), 351. https://doi.org/10.1130/G24435A.110.1130/2008088.
Qian, X., Feng, Q., Yang, W., Wang, Y., Chonglakmani, C., Monjai, D., 2015. Arc-like volcanic rocks in NW Laos: Geochronological and geochemical constraints and their tectonic implications. J. Asian Earth Sci. 98, 342–357. https://doi.org/10.1016/j.jseaes.2014.11.035.
Qian, X., Feng, Q., Wang, Y., Chonglakmani, C., Monjai, D., 2016. Geochronological and geochemical constraints on the mafic rocks along the Luang Prabang zone: Carboniferous back-arc setting in northwest Laos. Lithos 245, 60–75.
Rapp, R.P., Watson, E.B., 1995. Dehydration Melting of Metabasalt at 8–32 kbar: Implications for Continental Growth and Crust-Mantle Recycling. J. Petrol. 36 (4), 891–931. https://doi.org/10.1093/petrology/36.4.891.
Rapp, R.P., Shimizu, N., Norman, M.D., Applegate, G.S., 1999. Reaction between slab-derived melts and peridotite in the mantle wedge: experimental constraints at 3.8 GPa. Chem. Geol. 160 (4), 335–356.
Ridolfi, F., Renzulli, A., Puerini, M., 2010. Stability and chemical equilibrium of amphibole in calc-alkaline magmas: an overview, new thermobarometric formulations and application to subduction-related volcanoes. Contrib Mineral Petrol 160 (1), 45–66. https://doi.org/10.1007/s00410-009-0465-7.
Ridolfi, F., Renzulli, A., 2012. Calcic amphiboles in calc-alkaline and alkaline magmas: thermobarometric and chemometric empirical equations valid up to 1,130°C and 2.2 GPa. Contrib Mineral Petrol 163 (5), 877–895. https://doi.org/10.1007/s00410-011-0704-6.
Rollinson, H.R., 1993. Using geochemical data: evaluation, presentation, interpretation. Longman Scientific & Technical.
Rollinson, H., 2009. New models for the genesis of plagiogranites in the Oman ophiolite. Lithos, The genesis and significance of adakitic, high-Mg andesites, and other refractory magmas in intra-oceanic forearc settings 112 (3-4), 603–614. https://doi.org/10.1016/j.lithos.2009.06.006.
Rosenbaum, G., Sandiford, M., Caulfield, J., Garrison, J.M., 2018. A trapdoor mechanism for slab tearing and melt generation in the northern Andes. Geology 47, 23–26. https://doi.org/10.1130/G45429.1.
Rubatto, D., 2002. Zircon trace element geochemistry: partitioning with garnet and the link between U-Pb ages and metamorphism. Chem. Geol. 184 (1-2), 123–138. https://doi.org/10.1016/S0009-2541(01)00355-2.
Rudnick, R.L., Gao, S., 2003. Composition of the Continental Crust. Treatise on Geochemistry. Elsevier 1–64.
Salam, A., Khin Zaw, Meffre, S., McPhie, J., Lai, C.-K., 2014. Geochemistry and geochronology of the Chatree epithermal gold–silver deposit: Implications for the tectonic setting of the Loei Fold Belt, central Thailand. Gondwana Res. 26 (1), 198–217. https://doi.org/10.1016/j.gr.2013.10.008.
Salters, V.J.M., Stracke, A., 2004. Composition of the depleted mantle. Geochem. Geophys. Geosyst. 5 (5), n/a–n/a. https://doi.org/10.1029/2003GC000597.
Sashida, K., Igo, H., Adachi, S., Ueno, K., Kajiwara, Y., Nakornsri, N., Sardsud, A., 2000. Late Permian to Middle Triassic radiolarian faunas from northern Thailand. J. Paleontol. 74, 789–811. https://doi.org/10.1666/0022-3360(2000)074<0789:LPTMTR>2.0.CO;2.
Sashida, K., Salyapongse, S., 2002. Permian radiolarian faunas from Thailand and their paleogeographic significance. Journal of Asian Earth Sciences, Permian of Southeast Asia 20 (6), 691–701. https://doi.org/10.1016/S1367-9120(02)00005-6.
Şengör, A.M.C., Yılmaz, Y., Sungurlu, O., 1984. Tectonics of the Mediterranean Cimmerides: nature and evolution of the western termination of Palaeo-Tethys. Geological Society, London, Special Publications 17 (1), 77–112. https://doi.org/10.1144/GSL.SP.1984.017.01.04.
Shi, M., Khin Zaw, Liu, S., Xu, B., Meffre, S., Cong, F., Nie, F., Peng, Z., Wu, Z., 2021. Geochronology and petrogenesis of Carboniferous and Triassic volcanic rocks in NW Laos: Implications for the tectonic evolution of the Loei Fold Belt. J. Asian Earth Sci. 208, 104661 https://doi.org/10.1016/j.jseaes.2020.104661.
Sisson, T.W., Ratajeski, K., Hankins, W.B., Glazner, A.F., 2005. Voluminous granitic magmas from common basaltic sources. Contrib. Mineral. Petrol. 148 (6), 635–661. https://doi.org/10.1007/s00410-004-0632-9.
Smithies, R.H., 2000. The Archaean tonalite–trondhjemite–granodiorite (TTG) series is not an analogue of Cenozoic adakite. Earth Planet. Sci. Lett. 182 (1), 115–125. https://doi.org/10.1016/S0012-821X(00)00236-3.
Sone, M., Metcalfe, I., 2008. Parallel Tethyan sutures in mainland Southeast Asia: New insights for Palaeo-Tethys closure and implications for the Indosinian orogeny. Comptes Rendus Geoscience, L'orogénèse triasique indosinienne en Asie de l'Est 340 (2-3), 166–179. https://doi.org/10.1016/j.crte.2007.09.008.
Sone, M., Metcalfe, I., Chaodumrong, P., 2012. The Chanthaburi terrane of southeastern Thailand: Stratigraphic confirmation as a disrupted segment of the Sukhothai Arc. Journal of Asian Earth Sciences, Geological Anatomy of East and South Asia 61, 16–32. https://doi.org/10.1016/j.jseaes.2012.08.021.
Stern, C.R., Kilian, R., 1996. Role of the subducted slab, mantle wedge and continental crust in the generation of adakites from the Andean Austral Volcanic Zone. Contrib Mineral Petrol. 123 (3), 263–281.
Sun, S.-s., McDonough, W.F., 1989. Chemical and isotopic systematics of oceanic basalts: implications for mantle composition and processes. Geological Society, London, Special Publications 42 (1), 313–345. https://doi.org/10.1144/GSL.SP.1989.042.01.19.
Sun, Z.-M., Wang, X.-L., Zhang, F.-F., Xie, H.-Q., Zhao, K., Li, J.-Y., 2020. Diversity of Felsic Rocks in Oceanic Crust: Implications From the Neoproterozoic Plagiogranites Within the Northeast Jiangxi Ophiolite, Southern China. Journal of Geophysical Research: Solid Earth 125, e2019JB017414. https://doi.org/10.1029/2019JB017414.
Turner, S.J., Langmuir, C.H., 2015. What processes control the chemical compositions of arc front stratovolcanoes? Geochem. Geophys. Geosyst. 16 (6), 1865–1893. https://doi.org/10.1002/2014GC005633.
Ueno, K., Hisada, K.-I., 2001. The Nan-Uttaradit-Sa Kaeo Suture as a Main Paleo-Tethyan Suture in Thailand: Is it Real? Gondwana Res. 4 (4), 804–806. https://doi.org/10.1016/S1342-937X(05)70590-6.
Ueno, K., Miyahigashi, A., Charoentitirat, T., 2010. The Lopingian (Late Permian) of mid-oceanic carbonates in the Eastern Palaeotethys: stratigraphical outline and foraminiferal faunal succession. Geol. J. 45, 285–307. https://doi.org/10.1002/gj.1234.
Valley, J.W., 2003. Oxygen Isotopes in Zircon. Rev. Mineral. Geochem. 53 (1), 343–385. https://doi.org/10.2113/0530343.
Valley, J.W., Kinny, P.D., Schulze, D.J., Spicuzza, M.J., 1998. Zircon megacrysts from kimberlite: oxygen isotope variability among mantle melts. Contrib. Mineral. Petrol. 133 (1-2), 1–11. https://doi.org/10.1007/s004100050432.
Vervoort, J.D., Plank, T., Prytulak, J., 2011. The Hf–Nd isotopic composition of marine sediments. Geochim. Cosmochim. Acta 75 (20), 5903–5926. https://doi.org/10.1016/j.gca.2011.07.046.
Wai-Pan Ng, S., Chung, S.-L., Robb, L.J., Searle, M.P., Ghani, A.A., Whitehouse, M.J., Oliver, G.J.H., Sone, M., Gardiner, N.J., Roselee, M.H., 2015a. Petrogenesis of Malaysian granitoids in the Southeast Asian tin belt: Part 1. Geochemical and Sr-Nd isotopic characteristics. GSA Bulletin 127 (9-10), 1209–1237. https://doi.org/10.1130/B31213.110.1130/2015108.
Wai-Pan Ng, S., Whitehouse, M.J., Searle, M.P., Robb, L.J., Ghani, A.A., Chung, S.-L., Oliver, G.J.H., Sone, M., Gardiner, N.J., Roselee, M.H., 2015b. Petrogenesis of Malaysian granitoids in the Southeast Asian tin belt: Part 2. U-Pb zircon geochronology and tectonic model. GSA Bulletin 127 (9-10), 1238–1258. https://doi.org/10.1130/B31214.110.1130/2015121.

Wang, B.D., Wang, L., Chen, J., Liu, H., Yin, F., Li, X., 2017. Petrogenesis of Late Devonian-Early Carboniferous volcanic rocks in northern Tibet: New constraints on the Paleozoic tectonic evolution of the Tethyan Ocean. Gondwana Research, Tectonic evolution and dynamics of the Tibetan Plateau 41, 142–156. https://doi.org/10.1016/j.gr.2015.09.007.

Wang, B.D., Wang, L.Q., Pan, G.T., Yin, F.G., Wang, D.B., Tang, Y., 2013. U-Pb zircon dating of Early Paleozoic gabbro from the Nantinghe ophiolite in the Changning-Menglian suture zone and its geological implication. Chin. Sci. Bull. 58 (8), 920–930.

Wang, C., Deng, J., Santosh, M., Lu, Y., McCuaig, T.C., Carranza, E.J.M., Wang, Q., 2015. Age and origin of the Bulangshan and Mengsong granitoids and their significance for post-collisional tectonics in the Changning-Menglian Paleo-Tethys Orogen. Journal of Asian Earth Sciences, The Making of Asia 113, 656–676. https://doi.org/10.1016/j.jseaes.2015.05.001.

Wang, F., Liu, F.L., Liu, P.H., Shi, J.R., Cai, J., 2014. Petrogenesis of Lincang granites in the south of Lancangjiang area: Constrain from geochemistry and zircon U-Pb geochronology. Acta Petrologica Sinica 30, 3034–3050 in Chinese with English abstract.

Wang, H., Liu, F., Santosh, M., Wang, F., 2020a. Subduction erosion associated with Paleo-Tethys closure: Deep subduction of sediments and high pressure metamorphism in the SE Tibetan Plateau. Gondwana Res. 82, 171–192. https://doi.org/10.1016/j.gr.2020.01.001.

Wang, H., Liu, F., Sun, Z., Ji, L., Cai, J., Zhu, J., 2021. Identification of continental-type eclogites in the Paleo-Tethyan Changning-Menglian orogenic belt, southeastern Tibetan Plateau: Implications for the transition from oceanic to continental subduction. Lithos 396-397, 106215. https://doi.org/10.1016/j.lithos.2021.106215.

Wang, S., Mo, Y., Wang, C., Ye, P., 2016a. Paleotethyan evolution of the Indochina Block as deduced from granites in northern Laos. Gondwana Res. 38, 183–196. https://doi.org/10.1016/j.gr.2015.11.011.

Wang, Y.J., He, H., Cawood, P.A., Srithai, B., Feng, Q., Fan, W., Zhang, Y., Qian, X., 2016b. Geochronological, elemental and Sr-Nd-Hf-O isotopic constraints on the petrogenesis of the Triassic post-collisional granitic rocks in NW Thailand and its Paleotethyan implications. Lithos 266–267, 264–286. https://doi.org/10.1016/j.lithos.2016.09.012.

Wang, Y.J., Qian, X., Cawood, P.A., Liu, H., Feng, Q., Zhao, G., Zhang, Y., He, H., Zhang, P., 2018. Closure of the East Paleotethyan Ocean and amalgamation of the Eastern Cimmerian and Southeast Asia continental fragments. Earth-Science Reviews, Reconstruction of East Asian Continental Blocks in Pangea 186, 195–230. https://doi.org/10.1016/j.earscirev.2017.09.013.

Wang, Y., Yang, T., Zhang, Y., Qian, X., Gan, C., Wang, Y., Wang, Y., Seneboutalath, V., 2020b. Late Paleozoic back-arc basin in the Indochina block: Constraints from the mafic rocks in the Nan and Luang Prabang tectonic zones, Southeast Asia. J. Asian Earth Sci. 195, 104333. https://doi.org/10.1016/j.jseaes.2020.104333.

Wei, Y., Zi, J.-W., Liu, G., Sun, Z., Chen, G., Zhao, T., Nie, X., Yang, Z., 2022. Reconstructing the Lancang Terrane (SW Yunnan) and implications for early Paleozoic Proto-Tethys evolution at the northern margin of Gondwana. Gondwana Res. 101, 278–294. https://doi.org/10.1016/j.gr.2021.08.009.

Wonganan, N., Caridroit, M., 2007. Middle to Upper Permian radiolarian faunas from chert blocks in Pai area, northwestern Thailand. In: Baumgartner, P.O., Aitchison, J. C., De Wever, P., Jackett, S.-.-J. (Eds.), Radiolaria, Eclogae Geologicae Helvetiae Supplement. Birkhäuser, Basel, pp. 133–139. https://doi.org/10.1007/978-3-7643-8344-2_10.

Wu, F., Turner, S., Schaefer, B.F., 2020a. Mélange versus fluid and melt enrichment of subarc mantle: A novel test using barium isotopes in the Tonga-Kermadec arc. Geology 48 (11), 1053–1057. https://doi.org/10.1130/G47549.1.

Wu, F.-Y., Wan, B., Zhao, L., Xiao, W., Zhu, R., 2020b. Tethyan geodynamics. Acta Petrologica Sinica 36, 1627–1674 in Chinese with English abstract.

Yan, Y., Zhao, Q., Zhang, Y., Huang, B., Zheng, W., Zhang, P., 2019. Direct Paleomagnetic Constraint on the Closure of Paleo-Tethys and Its Implications for Linking the Tibetan and Southeast Asian Blocks. Geophys. Res. Lett. 46 (24), 14368–14376. https://doi.org/10.1029/2019GL085473.

Yang, W.-B., Niu, H.-C., Shan, Q., Sun, W.-D., Zhang, H., Li, N.-B., Jiang, Y.-H., Yu, X.-Y., 2014. Geochemistry of magmatic and hydrothermal zircon from the highly evolved Baerzhe alkaline granite: implications for Zr–REE–Nb mineralization. Miner Deposita 49 (4), 451–470. https://doi.org/10.1007/s00126-013-0504-1.

Zaw Myo Htet, 2021. Geology and mineral occurrences of Tachileik-Tar Lay Area, Tachileik and Tar Lay Townships, Shan State (East), Myanmar. Virtual GEOSEA XVI and GeoCon Conference, Abstract Volume, 6-8 December 2021, Philippines, p. 320.

Zhai, Q., Chung, S.-L., Tang, Y., Hu, P.-Y., Jin, X.-C., Wang, J., Wang, H.-T., Wang, K.-L., Lee, H.-Y., 2019. Late Carboniferous ophiolites from the southern Lancangjiang belt, SW China: Implication for the arc–back-arc system in the eastern Paleo-Tethys. Lithos 344–345, 134–146. https://doi.org/10.1016/j.lithos.2019.06.020.

Zhai, Q.-G., Jahn, B.-M., Wang, J., Hu, P.-Y., Chung, S.-L., Lee, H.-Y., Tang, S.-H., Tang, Y., 2016. Oldest Paleo-Tethyan ophiolitic mélange in the Tibetan Plateau. GSA Bulletin 128 (3-4), 355–373. https://doi.org/10.1130/B31296.110.1130/2015324.

Zhai, Q., Jahn, B., Wang, J., Su, L., Mo, X.-X., Wang, K., Tang, S., Lee, H., 2013. The Carboniferous ophiolite in the middle of the Qiangtang terrane, Northern Tibet: SHRIMP U-Pb dating, geochemical and Sr–Nd–Hf isotopic characteristics. Lithos 168–169, 186–199. https://doi.org/10.1016/j.lithos.2013.02.005.

Zhai, Q., Wang, J., Hu, P., Lee, H., Tang, Y., Wang, H., Tang, S., Chung, S., 2018. Late Paleozoic granitoids from central Qiangtang, northern Tibetan plateau: A record of Paleo-Tethys Ocean subduction. Journal of Asian Earth Sciences, Asian Orogeny and Continental Tectonics from Geochemical Perspectives. A Special Issue in Memory of Professor Bor-ming Jahn for His Scientific Contributions and Service (Part II) 167, 139–151. https://doi.org/10.1016/j.jseaes.2017.07.030.

Zhang, X., Chung, S.-L., Lai, Y.-M., Ghani, A.A., Murtadha, S., Lee, H.-Y., Hsu, C.-C., 2018. Detrital Zircons Dismember Sibumasu in East Gondwana. J. Geophys. Res. Solid Earth 123 (7), 6098–6110. https://doi.org/10.1029/2018JB015780.

Zhao, G., Wang, Y., Huang, B., Dong, Y., Li, S., Zhang, G., Yu, S., 2018. Geological reconstructions of the East Asian blocks: From the breakup of Rodinia to the assembly of Pangea. Earth-Science Reviews, Reconstruction of East Asian Continental Blocks in Pangea 186, 262–286. https://doi.org/10.1016/j.earscirev.2018.10.003.

Zhao, J., Huang, B., Yan, Y., Bai, Q., Dong, Y., Win, Z., Aung, H.H., Yang, X., Li, S., 2020. A palaeomagnetic study of the Middle Permian and Middle Triassic limestones from Shan State, Myanmar: Implications for collision of the Sibumasu Terrane and Indochina Terrane. Geol. J. 55 (2), 1179–1194. https://doi.org/10.1002/gj.3482.

Zi, J.-W., Cawood, P.A., Fan, W.-M., Wang, Y.-J., Tohver, E., 2012. Contrasting rift and subduction-related plagiogranites in the Jinshajiang ophiolitic mélange, southwest China, and implications for the Paleo-Tethys. Tectonics 31 (2), n/a–n/a. https://doi.org/10.1029/2011TC002937.

Zi, J.-W., Cawood, P.A., Fan, W.-M., Tohver, E., Wang, Y.-J., McCuaig, T.C., Peng, T.-P., 2013. Late Permian-Triassic magmatic evolution in the Jinshajiang orogenic belt, SW China and implications for orogenic processes following closure of the Paleo-Tethys. Am. J. Sci. 313 (2), 81–112. https://doi.org/10.2475/02.2013.02.

Zindler, A., Hart, S., 1986. Chemical Geodynamics. Annu. Rev. Earth Planet. Sci. 14 (1), 493–571. https://doi.org/10.1146/annurev.ea.14.050186.002425.